AD-A104 343 LOCKHEED MISSILES AND SPACE CO INC PALO ALTO CA PALO --ETC F/G 4/1
APPLICATION OF VISIBLE MONOCHROMATIC AURORAL IMAGING DATA FOR M--ETC(U)
JAN 81 J B KUMER, R D SEARS, J E EVANS F19628-78-C-0817
UNCLASSIFIED LMSC/D802558 AFGL-TR-81-0025 NL

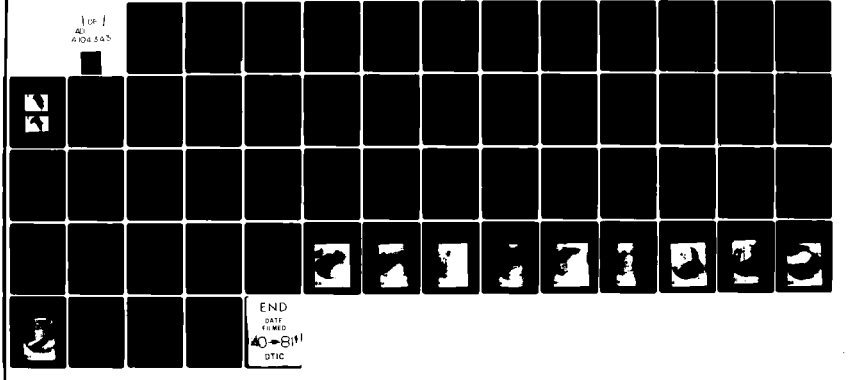

AFGL-TR-81-0025

APPLICATION OF VISIBLE MONOCHROMATIC AURORAL IMAGING DATA FOR MODELING INFRARED EARTH-LIMB MORPHOLOGY

J.B. Kumer
R.D. Sears
J.E. Evans
S.E. Harris
R.M. Nadile

Electro-Optics Laboratory
Lockheed Palo Alto Research Laboratories
Palo Alto, California 94304

Final Report
September 1978 - January 1981

26 January 1981

AIR FORCE GEOPHYSICS LABORATORY
AIR FORCE SYSTEMS COMMAND
UNITED STATES AIR FORCE
HANSCOM AFB, MASSACHUSETTS 01731

UNCLASSIFIED

SECURITY CLASSIFICATION OF THIS PAGE (When Data Entered)

19 REPORT DOCUMENTATION PAGE	READ INSTRUCTIONS BEFORE COMPLETING FORM
1. REPORT NUMBER: AFGL-TR-81-0025	2. GOVT ACCESSION NO.: AD-A104343
3. RECIPIENT'S CATALOG NUMBER: 9	
4. TITLE (and Subtitle): Application of Visible Monochromatic Auroral Imaging Data for Modeling Infrared Earth-Limb Morphology.	5. TYPE OF REPORT & PERIOD COVERED: Final Report. September 1978-January 1981
	6. PERFORMING ORG. REPORT NUMBER: LMSC / D802558
7. AUTHOR(s): J.B. Kumer, R.D. Sears, J.E. Evans, S.E. Harris, R.M. Nadile*	8. CONTRACT OR GRANT NUMBER(s): F19628-78-C-0217
9. PERFORMING ORGANIZATION NAME AND ADDRESS: Electro-Optics Laboratory, Lockheed Palo Alto Research Laboratories, Palo Alto, CA 94304	10. PROGRAM ELEMENT, PROJECT, TASK AREA & WORK UNIT NUMBERS: 61102F, 2310G4AL
11. CONTROLLING OFFICE NAME AND ADDRESS: Air Force Geophysics Laboratory, Hanscom AFB, Massachusetts 01731, Monitor/Richard M. Nadile/OPR-1	12. REPORT DATE: 26 January 1981
	13. NUMBER OF PAGES: 57
14. MONITORING AGENCY NAME & ADDRESS (if different from Controlling Office)	15. SECURITY CLASS. (of this report): UNCLASSIFIED
	15a. DECLASSIFICATION/DOWNGRADING SCHEDULE

16. DISTRIBUTION STATEMENT (of this Report)

Approved for public release; distribution unlimited.

17. DISTRIBUTION STATEMENT (of the abstract entered in Block 20, if different from Report)

18. SUPPLEMENTARY NOTES

*AFGL, Hanscom AFB, Massachusetts 01731

19. KEY WORDS (Continue on reverse side if necessary and identify by block number)

Earth limb, Infrared, Structure, Aurora, Temporal, All-sky television data, Earth-limb radiance, Radiance modelling, Auroral emissions, CO_2 4.3 μm Emission, ICECAP, HAES, Auroral 4278-Å emission, Auroral 6300-Å emission, Prompt 4.3-μm auroral emission.

20. ABSTRACT (Continue on reverse side if necessary and identify by block number)

A statistically comprehensive first-order auroral earth-limb data base at 2.7 and 4.3 μm is constructed from an existing 4278 and 6300 Å, ground-based, all-sky TV data base, which includes approximately 200 hours of all-sky auroral data that are stored on video tape. Methods of modeling 2.7- and 4.3-μm auroral emissions on the basis of measurements of the aurora in the spectral regions

(Continued on backside of form)

DD FORM 1 JAN 73 1473 EDITION OF 1 NOV 65 IS OBSOLETE

UNCLASSIFIED

SECURITY CLASSIFICATION OF THIS PAGE (When Data Entered)

(4278 Å) and (6300 Å) have been developed and verified against infrared data. 2.7-μm emission is modeled by the $N(^2D) + O_2 \rightarrow NO + O$ mechanism. The 4.3-μm emission is modeled by two mechanisms, a relatively slower (5 to 25 min response time) mechanism due to emission by CO_2, and a weaker but fast (1 to 10 s) mechanism that is indicated by the auroral data obtained 26 October 1978. In this effort, approximately 30 min of real-time auroral all-sky video data from each of the events 3/23/73 and 3/27/73 were digitized. The digitized data from the 3/23/73 event were used to construct a dynamic 2-dimensional model of auroral 2.7 and 4.3 μm earth-limb radiance over the 30 min observation period. It is seen that structure is more prominent for the relatively fast 2.7- and 4.3-μm mechanisms than for the slower CO_2 4.3-μm mechanism.

ABSTRACT

A statistically comprehensive first-order auroral earth-limb data base at 2.7 and 4.3 μm is constructed from an existing 4,278- and 6,300-Å, ground-based, all-sky TV data base, which includes approximately 200 hours of all-sky auroral data that are stored on video tape. Methods of modeling 2.7- and 4.3-μm auroral emissions on the basis of measurements of the aurora in the spectral regions (4,278 Å) and (6,300 Å) have been developed and verified against infrared data. 2.7-μm emission is modeled by the $N(^2D) + O_2 \rightarrow NO + O$ mechanism. The 4.3-μm emission is modeled by two mechanisms, a relatively slower (5- to 25-min response time) mechanism due to emission by CO_2, and a weaker but fast (1- to 10-s) mechanism that is indicated by the auroral data obtained 26 October 1978. Structure is more prominent for the relatively fast 2.7- and 4.3-μm mechanisms than for the slower CO_2 4.3-μm mechanism.

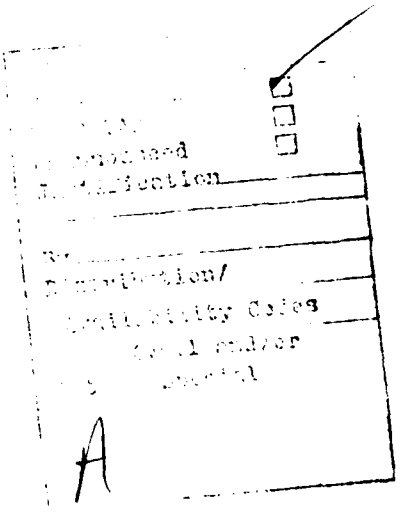

CONTENTS

ILLUSTRATIONS

TABLES

Section 1
INTRODUCTION

We describe an effort to construct a first-order auroral earth-limb data base at 2.7 and 4.3 μm from an extensive all-sky television (TV) data base which has been obtained in a series of field operations beginning in 1972. The TV data base includes more than 200 hours of all-sky multispectral image intensified TV imaging data of aurora and airglow which have been taken and stored on video tape by LMSC personnel (S. B. Mende and R. D. Sears) since 1972. We have used some of these data to construct morphological models of the auroral earth-limb infrared radiance, as it would be sensed by a high-altitude, satellite-borne sensor, in the spectral regions of atmospheric absorption near 2.7 and 4.3 μm.

Research performed under the DNA/AFGL auroral measurements program has shown that there are strong auroral emissions near 2.7 and 4.3 μm. Methods for modeling (blue red input model, BRIM) these infrared emissions on the basis of ground-based photometric measurements of the aurora in the spectral regions blue (4,278 Å) and red (6,300 Å) have been developed and verified against infrared data which were obtained simultaneously via rocket-borne, zenith-viewing sensors. These methods are discussed in a report by Kumer (Ref. 1).

In this report we discuss the use of the BRIM capability to construct images of the infrared earth-limb radiance from successive pairs of blue and red all-sky TV images. The successive TV images are obtained at a rate of approximately once every 15 s or faster. Thus, it is possible to use the TV data to generate a series of infrared earth-limb radiance images which will demonstrate the dynamic behavior of the infrared earth limb with time resolution of at least 15 s. The spatial resolution of the TV is such that structure on the scale of several km may be resolved in the infrared earth-limb radiance images. The all-sky TV coverage has a zenith full cone angle of 140 deg. This is extensive enough that earth-limb infrared images of horizontal extent of up to 700 km and tangent altitude extent from 40 to 140 km may be constructed. Spatial power spectral densities (PSDs) may be obtained from the earth-limb radiance images. Temporal PSDs may be obtained from a series of earth-limb infrared images.

Section 2 of this report discusses the details of our all-sky multispectral image intensified TV auroral data base and our system for digitizing and calibrating these data. Section 3 reviews the physics that allows us to generate three-dimensional infrared volume emission rates from the two-dimensional blue and red TV data. Section 4 outlines the data processing and computational aspects of the project. The computational techniques were developed and verified by application to simulated TV imaging data and then were applied to about 200 frames of TV imaging data from observations in Alaska in 1973. By inspection of a sample of these results it is apparent that the spatial and temporal structure in the auroral CO_2 4.3-μm earth limb is milder than that in the auroral 2.7-μm earth limb.

Nominally, the final product of the project could include 2.7- and 4.3-μm earth-limb images computed for a comprehensive selection of auroral events as listed in Table 1-1. The images may be constructed as a function of space and time. Table 1-1 also lists the nominal amounts of real-time data and TV frames that may be processed for each type of event.

Table 1-1 TYPES OF AURORAL EVENTS AND NOMINAL QUANTITIES OF DATA TO BE PROCESSED

Event	Real Time (min)	Number of Pairs of Blue and Red TV Frames
Breakup with Surge	20	240
Single Moving Arc	10	60
Multiple Moving Arcs	10	60
Diffuse Aurora	5	20
Flaming Aurora	10	60
Pulsating Aurora	10	60

Section 2
MONOCHROMATIC AURORAL ALL-SKY TV CAMERA AND AVAILABLE DATA BASE

All-sky monochromatic auroral TV images have been recorded on various occasions during the past few years, using an image intensified TV camera sensor system devised by S. B. Mende and R. H. Eather (Ref. 2). The auroral imaging system records sequences of all-sky images on magnetic video tape in a timelapse format such that an entire night's observations can be accommodated on one or two tapes. A "bar coded" representation of local time, wavelength, and exposure time is included in each image. Auroral images are obtained in the wavelengths 4,278 and 6,300 Å, which are used for the analysis we report here, and in the 4,861 H_b emission line and a background band centered at 4,831 Å. Depending on auroral intensity, exposure (or integration) times of up to a few seconds and total sequence times up to 10 to 15 s or so are typical. Thus, auroral structure in a given wavelength can be monitored in time with a frame sequence time of about 15 s or shorter. A sample of successive blue and red frames of multiple auroral arcs obtained 23 March 1973 is shown in Fig. 2-1. This figure illustrates the form of the video images and the placement of the "bar coded" information. To date, many hours of this type of data on a wide variety of auroral conditions have been obtained.

The data base includes auroral imagery from field programs conducted during 1973 in Chatanika, Alaska; 1975 in Gillam, Manitoba; 1976 in Kiruna, Sweden; and 1980 in Siple Station, Antarctica. During the 1973 experimental period, the TV system was operated at the LMSC optical research site at Chatanika in close coordination with photometric observations that were obtained simultaneously with AFGL/DNA ICECAP rocketborne infrared experiments. Table 2-1 lists the Chatanika observations in 1973. In all cases the TV data were obtained simultaneously with ground-based photometric data. These data are carefully calibrated and are used to assist in calibration and interpretation of the all-sky TV imagery.

In this effort we achieved digitization of 1973 data, which included most of the phenomena listed in Table 2-1. A Colorado Video (Model 240) frame storer is used to digitize and store TV frames (256 by 256 8-bit samples); this unit

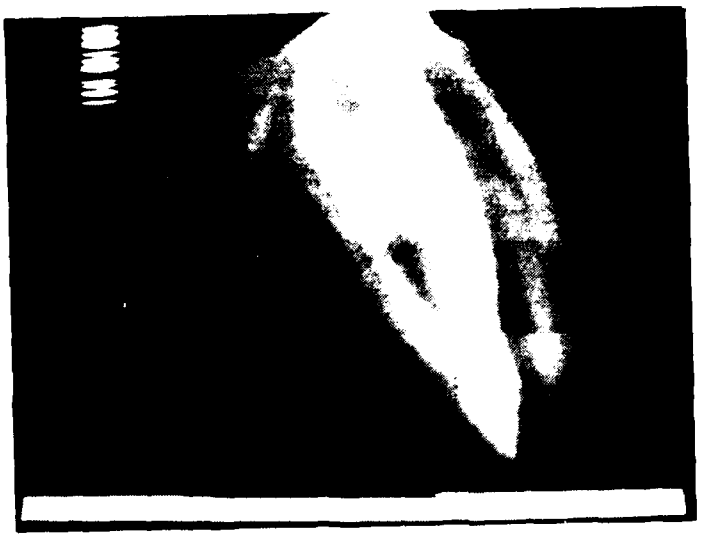

Blue

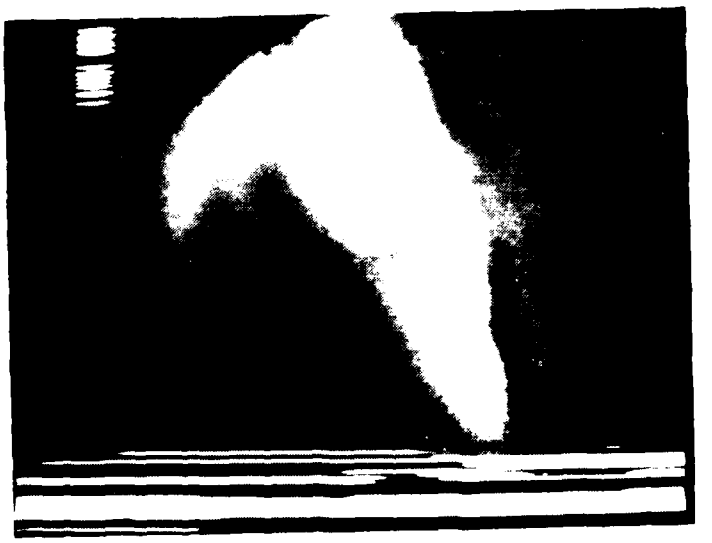

Red

Fig. 2-1 Sample Blue and Red Pair Frame Obtained March 1973

Table 2-1 LIST OF CHATANIKA, 1973 OBSERVATIONS(a)

Tape	Date	Start Time	Stop Time
1	3-22-73	(b)	2245
2	3-22-73	(b)	2400
3	3-23-73	0040	0115
4	3-24-73	Morning(b)	Paiute Tomahawk
5	3-24-73	App. 2100, Evening	(b)
6	3-24-73	Evening	(b)
7	3-25-73	2100	2200
8	3-25-73	2200	2300
9	3-27-73	2142	2242
10	3-27-73	2242	2342
11	3-27-73	2342	(b)
12	3-28-73	2100	2200
13	3-30-73	0047	0147
14	3-30-73	0047	0147
15	3-30-73	(b)	0255
16	3-30-73	2216	2320
17	3-31-73	0055	0155

(a) Each video tape lasts approximately 1 h.
Exact time can be established by decoding the time.
All dates and times are local.
(b) Exact time is available on demand.

is interfaced with a monitor, a Data General NOVA 3 minicomputer system, and a tape drive unit (9 track, 800 bpi). The system also includes a CRT terminal, a Bell-Howell CEC 912 gray scale hard copy unit, and a printer unit. A schematic of tne digitization system is shown in Fig. 2-2. The data in Fig. 2-1 are velox reproductions of photographs of the frame storer monitor display of the digitized data in the frame storer for a sample pair of consecutive red and blue video data frames obtained 23 March 1973. The NOVA software provides for interfacing the frame storer data with the tape drive, decoding the bar pattern to provide identification for the digitized TV data frames, miss-synchronization position corrections for the digitized TV frame, suppression of saturation effects in the digitized data, and use of the simultaneously acquired calibrated photometric data in order to apply firm calibration to the TV data.

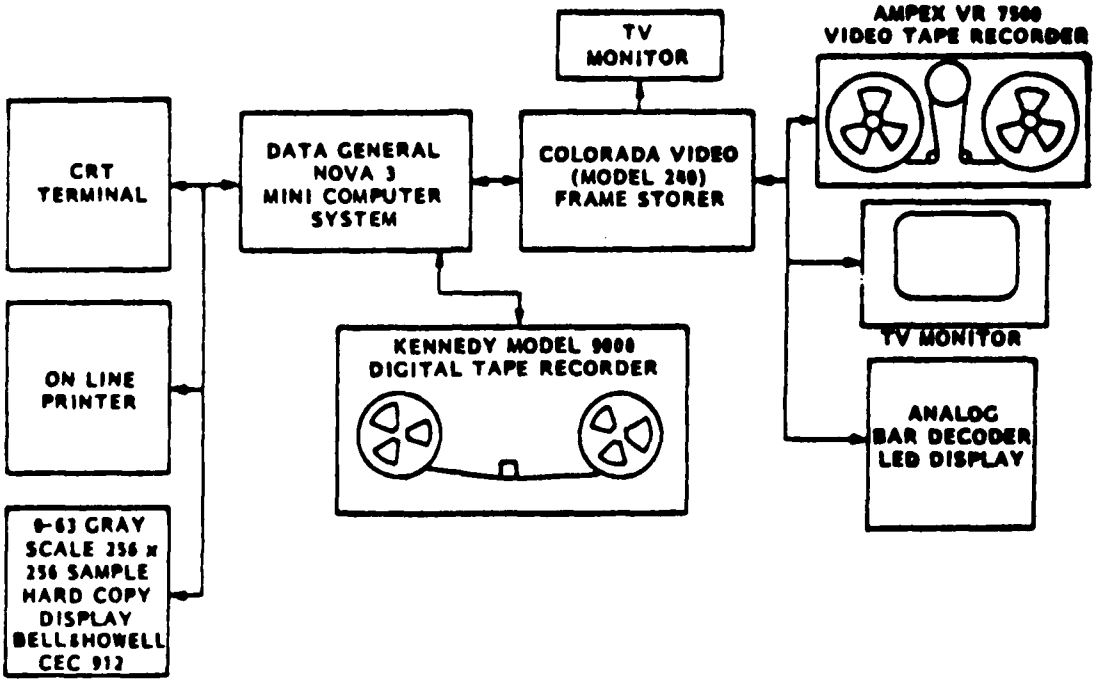

Fig. 2-2 Schematic of TV Digitization System

Section 3
COMPUTATION OF INFRARED VOLUME EMISSION FROM BLUE (4,278 Å) AND RED (6,300 Å) TV DATA

3.1 BACKGROUND

Methods that may be inferred from the work reported by Rees and Luckey (Ref. 3) may be used to approximately construct an instantaneous energy deposition rate profile q(z,t) from the TV brightness data which are measured in narrow spectral bands in the blue (4,278 Å) and in the red (6,300 Å) spectral region. The blue data $4\pi I_B(t)$ are proportional to the height integrated energy deposition rate $\int dz\, q(z,t)$, and the ratio I_B/I_R of the blue to red may be associated with the altitude Z_p, where q is a maximum if one assumes that the energy dependence of the incident electrons takes the form $\phi = \phi_0 E \exp(-E/\alpha)$.

In a recent paper Sears (Ref. 4) has reviewed the theoretical and technological basis for inferring properties of the auroral ionosphere (i.e., energy deposition rate, ion pair production rate, electron density, etc.) from ground-based observations of visible auroral emissions, including the red and blue emissions as discussed above. Other verification that visible measurements may be used to infer auroral ionospheric and atmospheric parameters have been published by Wickwar, Baron, and Sears (Ref. 5) and by Vondrak and Sears (Ref. 6). It is not surprising, then, that Kumer (Ref. 1) has shown that auroral blue and red measurements may also be used to model auroral infrared emissions, since these also critically depend on the time history of the altitude distribution of auroral energy deposit. This application is described by Kumer (Ref. 1) in HAES report 57, where he discusses the method (blue red input model, BRIM) for approximately constructing a deposition profile q(z,t) from the blue and red brightness data $4\pi I_B$ and $4\pi I_R$. In this report application of the BRIM model for analysis of 4.3-μm auroral zenith radiance data that were obtained 25 February 1974 and 12 March 1975 is considered. Good agreement was obtained between the 4.3-μm data and the BRIM-model predictions, thus providing a verification of the utility of BRIM for modeling the infrared aurora.

An example of the comparison between the upleg and downleg BRIM calculations for 4.3-μm zenith radiance and the data obtained in the case of the 25 February 1974 auroral event are shown in Figs. 3-1 and 3-2. Ground-based photometric red and blue auroral data taken at the point of upleg and downleg penetration at 80 to 110 km are listed in Table 3-1. The auroral photometric red and blue data are input to the BRIM model; the resultant agreement between the BRIM predictions and the 4.3-μm data is clearly illustrated by Figs. 3-1 and 3-2. Similar success has been obtained by application of the BRIM model, using red and blue input data, to analyze 4.3-μm auroral data obtained on many other occasions (12 March 1975, 24 March 1973, and 26 October 1978 are notable but not exhaustive samples).

Table 3-1 THE OBSERVED HISTORIES OF RED AND BLUE AURORAL BRIGHTNESS [$4\pi I_R'$ at 6,300 Å and $4\pi I_B'$ at 3,914 Å (Ref. 7)]for the 25 February 1974 upleg and downleg penetration (80 to 110 km) are listed in below. The time t' is measured backwards from rocket penetration time. The auroral 4.3-μm response time is of the order 5 min or more; this requires the photometric history to exist for many minutes prior to penetration in order to accurately model the 4.3-μm data.

Upleg			Downleg		
minutes	kR		minutes	kR	
t'	$4\pi I_R'$	$4\pi I_B'$	t'	$4\pi I_R'$	$4\pi I_B'$
0.	1.2	10.0	0.	1.1	6.0
0.9	1.3	23.0	0.88	1.3	20.0
2.03	2.8	53.0	1.33	2.1	115.0
2.28	2.1	53.0	1.83	1.0	10.0
3.15	1.6	32.0	2.67	0.8	6.0
3.62	2.2	45.0	3.57	1.2	11.0
4.28	1.5	16.0	4.03	2.7	57.0
4.97	1.2	16.0	6.17	2.2	11.0
5.20	1.4	6.0	6.85	1.6	6.0
6.10	0.8	3.0	11.00	0.6	2.0

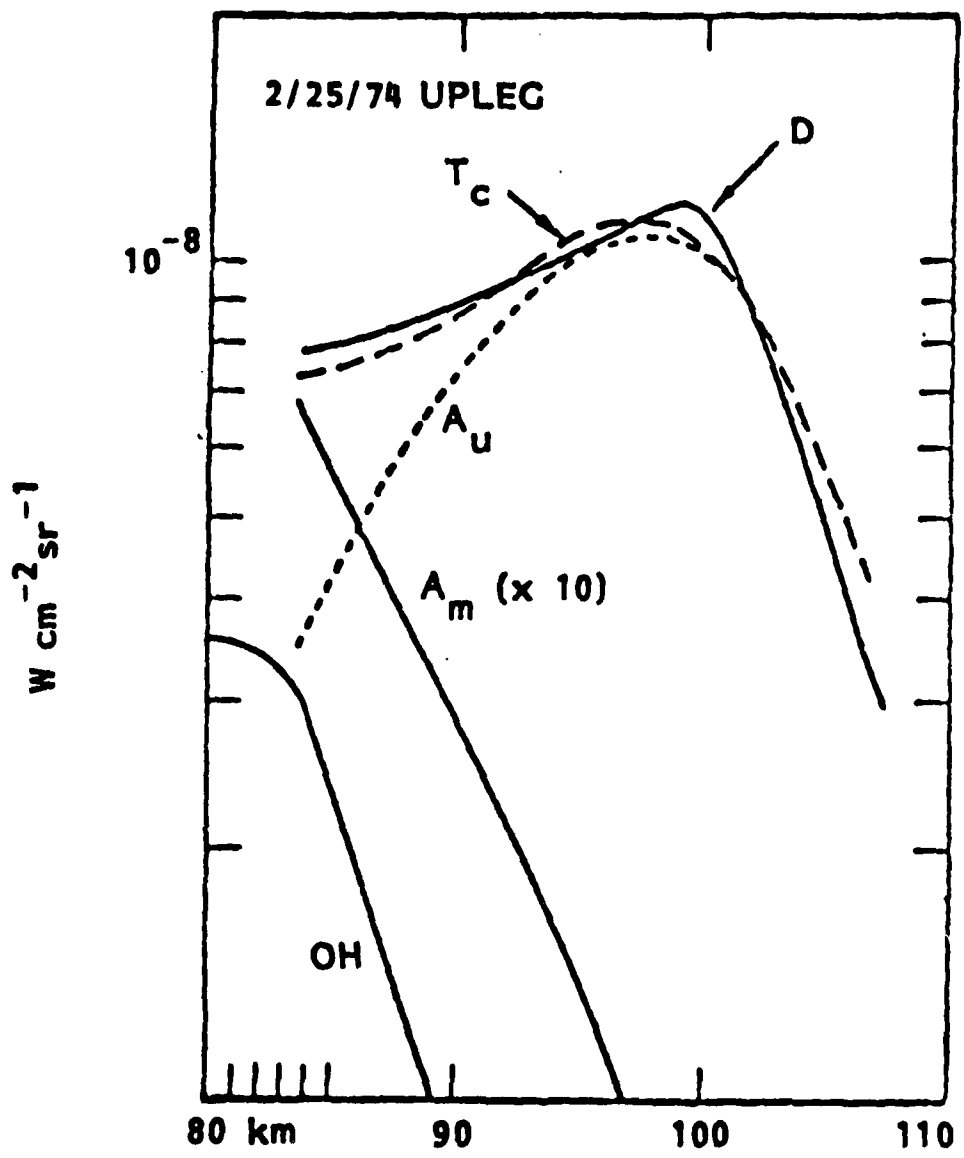

Fig. 3-1 25 February 1974 Upleg 4.3-μm Zenith Radiance Data (Curve D) are Compared With Curves A_u, the BRIM Calculation for the Auroral Component of Zenith Radiance; OH, the Calculated Component Due to Vibration Transfer From OH; A_m(x10), the Ambient Thermal Component Multiplied by a Factor 10 So That It Is on Scale; and T_c, the Sum OH + A_u + A_m

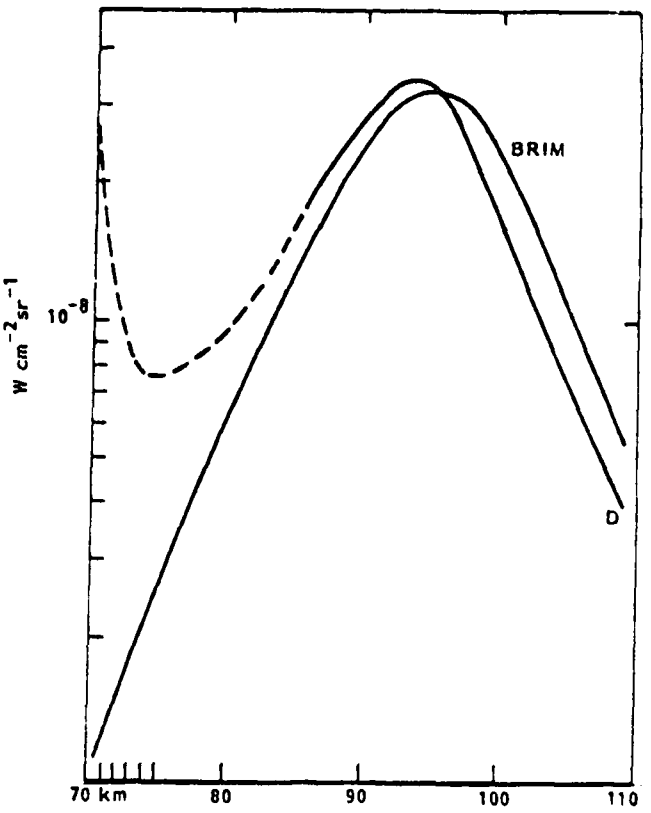

Fig. 3-2 Comparison of the 25 February 1974 Downleg Data (Curve D) and Calculations (Curve BRIM) Based on Our BRIM Model

3.2 IR EMISSION MECHANISM

For the purpose of calculating the 2.7-μm volume emission rate, we assume that the reaction $N(2_D) + O_2 \rightarrow NO(V) + O$ is the final chemical step in the production of auroral 2.7-μm volume emission. We use an energy efficiency $\epsilon_{2.7} \cong 0.7$ percent for the auroral production of 2.7-μm volume emission. The time constant $\tau_{2.7}$ for 2.7-μm volume emission is given by $\tau_{2.7} = (k_{2.7}[O_2])$, where $k_{2.7}$ is the rate constant for the time-limiting step $N(^2D) + O_2 \rightarrow NO(V) + O$. The maximum value we will be concerned with for $\tau_{2.7}$ is $\tau_{2.7} \cong 90$ s, which occurs at $z =$ 160-km altitude, the highest altitude that will concern us. This maximum value for $\tau_{2.7}$ is greater than a TV frame time, so we will have to pay some attention to the deposition time history even for the case of 2.7-μm volume emission. The 2.7-μm volume emission rate $\mathcal{E}_{2.7}(\vec{r},t)$ at point $\vec{r}$ and time t will be given by

The quantity $f(z)$ is defined on p. 31 of a Kumer report (Ref. 11). The quantities $\Omega(z)$ and $E(z)$ are defined in the paper by Kumer and James (Ref. 12), and Ω is modified by the Q_W approximation in order to account for the weak CO_2 bands as is discussed by Kumer (Ref. 10). The energy efficiency $\epsilon_{4.3}$ for auroral excitation of N_2 is taken to be $\epsilon_{4.3} = 10$ percent. The quantity $Q_{4.3}(\vec{r},t)$ is generated via

$$Q_{4.3}(\vec{r},t) = \exp(-\Delta t/\tau_{4.3})\ Q_{4.3}(\vec{r},t-\Delta t) + [1-\exp(-\Delta t/\tau_{4.3})]q(\vec{r},t) \tag{6}$$

The initial value $Q_{4.3}(\vec{r},t_0)$ will be selected in the same way that $Q_{2.7}(\vec{r},t_0)$ is selected, as discussed above.

The prompt emission observed in the 26 October 1978 4.3-μm auroral data (Refs. 8 and 9) is also included in the model. Presently, the process is characterized as prompt and 0.3-percent energy efficient above 110 km, but considerably less efficient below 110 km. More precise information on the characteristics of this relatively weak but prompt 4.3-μm auroral emission is expected to be obtained in the auroral field widened interferometer (FWI) and the ELIAS auroral earth-limb experiments that are currently scheduled for the 1981/1982 winter season. A prime candidate to explain the prompt mechanism is emission by $NO^+(V)$.

3.3 GEOMETRIC CONSIDERATIONS

Our purpose is to generate infrared earth-limb radiance pictures which may extend horizontally for several hundred km and in some cases as much as 100 km in tangent altitude Z_h, and to construct these pictures from ground-based, all-sky TV data, which are obtained in a zenith angle range from 0 to 77 deg. The TV coverage includes a horizontal radius of about 450 km from the camera. If we place the camera underneath the line-of-sight tangent point at 100 km alti-

$$\mathcal{E}_{2.7} = \epsilon_{2.7}\ Q_{2.7}(\vec{r},t) \tag{1}$$

where

$$Q_{2.7}(\vec{r},t) = \int_{-\infty}^{t} \frac{dt'}{\tau_{2.7}} \exp\left(-(t-t')\tau_{2.7}^{-1}\right) q(\vec{r},t') \tag{2}$$

For a frame at time t, we generate $Q_{2.7}(\vec{r},t)$ from the deposition $q(\vec{r},t)$ and from the time history $Q_{2.7}(\vec{r},t - \Delta t)$, which characterized the previous frame (at $t-\Delta t$) by

$$\begin{aligned} Q_{2.7}(\vec{r},t) = \exp(-\Delta t/\tau_{2.7})\ Q_{2.7}(\vec{r},t-\Delta t) \\ + \left(1-\exp(-\Delta t/\tau_{2.7})\right) q(\vec{r},t) \end{aligned} \tag{3}$$

One sees that at lower altitudes where $\tau_{2.7} << \Delta t$, that $Q_{2.7}(t) \cong q(t)$.

Initial values of $Q_{2.7}(t_0)$ for t_0, the time of the first frame in a series of frames to be processed, will be given by $Q_{2.7}(t_0) = q(t_0)$. This is equivalent to assuming steadystate conditions for $t < t_0$. This is reasonable, since t_0 may be selected such that events prior to t_0 may be uninteresting by comparison to events following t_0.

In the 4.3-μm region, two auroral mechanisms will be considered, namely, the "slow" ($4 < \tau_{4.3} < 20$ min) $N_2 \rightleftharpoons CO_2\ (\nu_3)$ mechanism, and a second nearly prompt (albeit, much weaker) mechanism that has been identified (Refs. 8 and 9) in auroral 4.3-μm data that were obtained 26 October 1978. The CO_2 4.3-μm volume emission rate $\mathcal{E}_{4.3}$ may be approximately calculated by the technique EFA, Q_W, that is given in a paper by Kumer (Ref. 10). In this approximation

$$\mathcal{E}_{4.3} \cong F(z)\ \epsilon_{4.3}\ Q_{4.3}(\vec{r},t) \tag{4}$$

where

$$F(z) = f(z)\left\{1 - \Omega(z)\,[1-E(z)]\right\}^{-1} \tag{5}$$

tude, as viewed from the satellite, then the light-emitting volumes along the LOS which samples the emission at 100-km altitude, 450 km from the TV station will sample the emission at 83-km altitude over the TV station. The geometry is illustrated by Fig. 3-3.

Points on the plane illustrated by Fig. 3-3 may be located by the coordinates S and Z_h, where S is measured from the tangent point along a satellite viewing line of sight (LOS) and where each LOS is characterized by Z_h, the altitude of the tangent point.

3.4 INITIAL DATA PROCESSING

The digitized TV data are stored on tape - one tape record/line of TV data. After calibration correction, these numbers are the $4\pi I_B$ and $4\pi I_R$ which were measured along the TV camera line of sight associated with the resolution point. The camera is normally set up so that the lines run in the magnetic north-south direction. Corresponding resolution points, on the blue and the

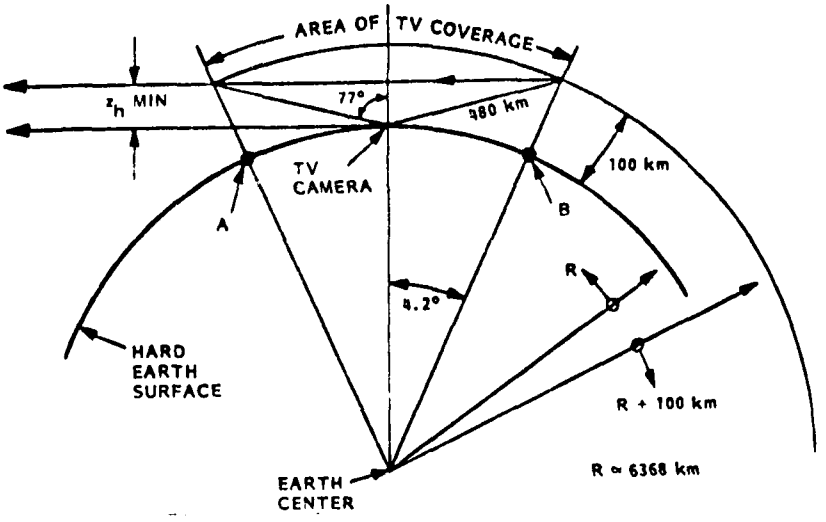

Fig. 3-3 TV Camera Positioned at the Hard Earth Line-of-Sight Tangent Point. The Minimum Value for Z_h for Auroral Emission at Z = 100 km is Z_h min = 83 km

red lines, are processed simultaneously. The ratio I_B/I_R gives the altitude Z_p of maximum deposition. This determines the range from the TV camera and thereby the horizontal coordinates (x, y) of the point. Since I_B/I_R may vary considerably along the line of TV data, the set of points traced out in this way will not in general form a smooth curve in physical space. Thus, each TV data line of points defines a physically irregular curve of horizontal points (x,y) which has a number pair of red and blue values (I_R, I_B) associated with each point. These irregular lines or bands form slightly distorted hyperbolic curves with the density of data points being much less at larger radii.

Figure 3-4 shows the distribution of data points in a subauroral plane from a grid of 256 x 256 points in the x, y plane for uniform altitude of maximum energy deposition Z_p = 110 km. Only data points from every eighth scan line and every eighth data point along scan lines are shown. Figure 3-5 shows how this regular distribution of Fig. 6 is affected by a simulated auroral scene containing auroral arcs. Data from a single magnetic meridian scan with 4,278- and 6,300-Å filtered photometer channels taken in Alaska by R. D. Sears on 26 October 1978, when there was a prominent arc present, were used as the basis for the simulated auroral scene. These scan patterns were projected east and west along lines of constant magnetic latitude, with a 20-km wavelength sine wave giving 30 percent modulation acting on the parallel scan patterns.

Major distortion to regular shaped curves can be observed in Fig. 3-5 along east-west lines (vertical lines on Fig. 3-5) near 325 km north, 40 km north, and 60 km south of the TV location.

The next step in the data processing is to determine for each data-point location (x,y) an index which is used to select those data points in a narrow band having a width of 2 km along the LOS that is to be selected, or calculated from a satellite ephemeris point and the coordinates of the TV observing station, for limb viewing of the auroral scene. Using the point-slope formula we calculate the x-axis intercept of a line through each point parallel to the LOS. All data points whose x-intercepts fall into a selected interval are located

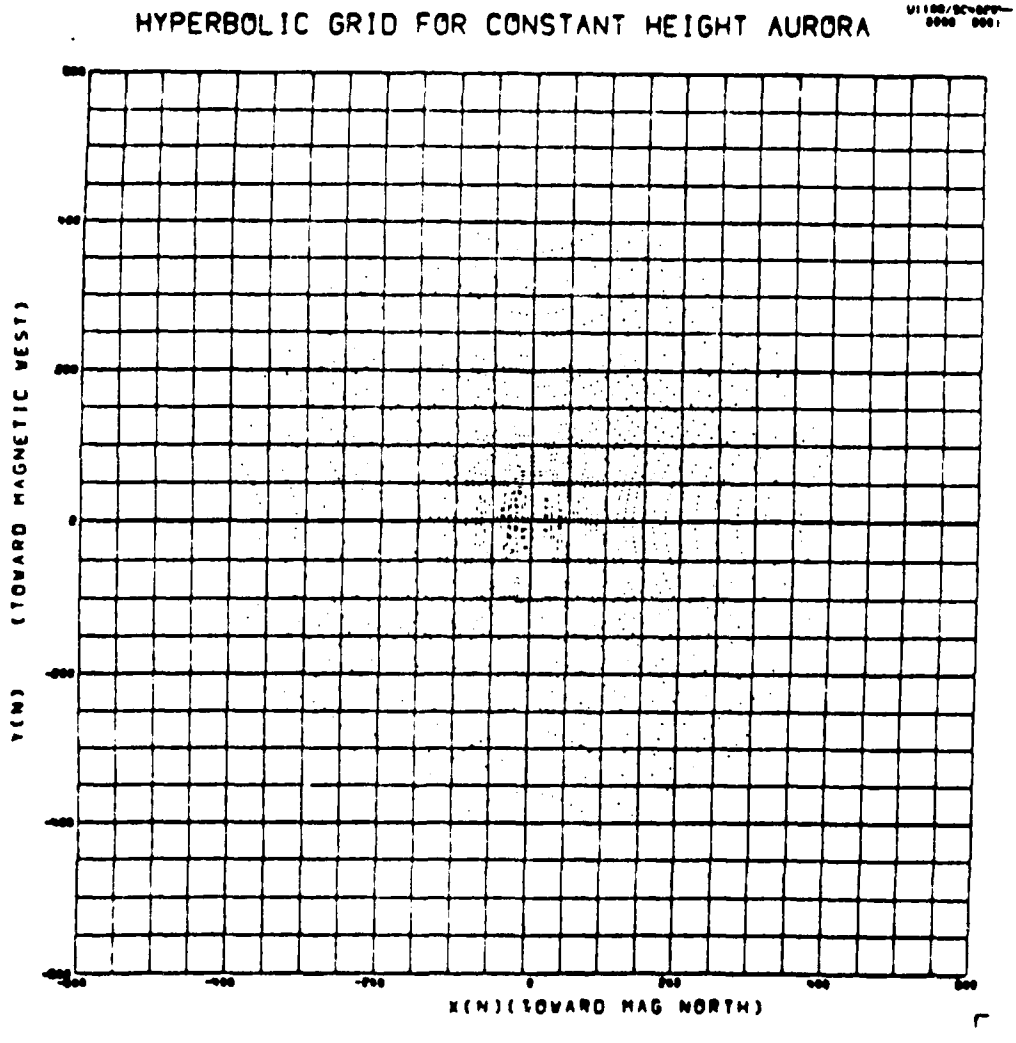

Fig. 3-4 Distribution of Data Point Locations on a Subauroral Plane Assuming a Constant Altitude of 110 km for Auroral Emission

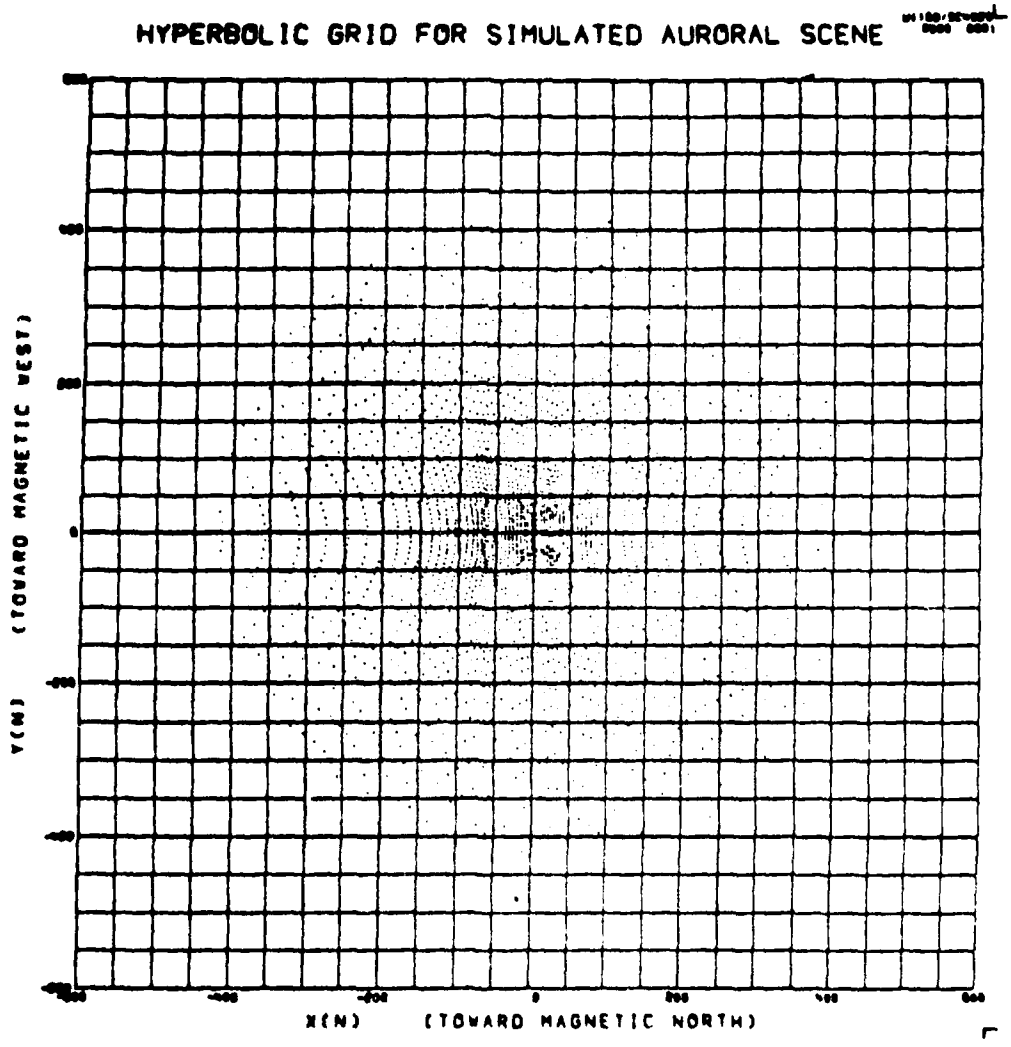

Fig. 3-5 Distribution of Data Point Locations on a Subauroral Plane Showing Distortion Effects of Varying Emission Altitudes, Such as Those Measured in Auroral Arcs

within the desired narrow band along the LOS. When the LOS is more than approximately 45 deg from the magnetic meridian, the y-axis intercept may be used. This selection process has reduced the number of data points from about 60,000 for the complete TV frame to about 8,000 points, which are included in the 2-km parallel strips along the 51 LOS. Three quantities associated with each data point are S, the coordinate that spatially locates the point along the satellite LOS, and the blue and red brightnesses, $4\pi I_B$ and $4\pi I_R$.

The data are coalesced into cells on the LOS with boundaries defined by equal TV zenith angle intervals (or other nonuniform or uniform intervals as desired). The equal steps of zenith angle are selected so that a nearby equal number N of data points are associated with each mesh point, S_i on a given LOS. When 100 mesh points are used, a resolution along the LOS of 2.7 km is obtained near the center for a tangent altitude of 100 km. Near the edge of the TV field the resolution will be about 40 km along the LOS. This simple scheme is appropriate if the most intense aurora are located approximately at the TV zenith. Once the cells have been selected, then the average red and/or blue brightness to be associated with a cell may be computed via

$$4\pi\bar{I} = \sum_{j=1}^{N} 4\pi I_j/N$$

3.5 EARTH-LIMB RADIANCE COMPUTATION

Figure 3-6 shows a plane containing a line-of-sight-having constant x. For our present geometry, the quantity $y = R_e\theta$ where R_e is the earth's radius and $0 \leq \theta \leq 8.4$ deg. In the previous section we explained how records of blue-red data pairs (I_B, I_R) would be generated for each plane defined by x. Approximately one-hundred such data pairs are included in each tape record. The energy deposit rates $q\ (z_h, S_i, t)$ for each cell along the LOS is computed at time t from the blue and red TV data as described above. The updated values for $Q_{2.7}\ (Z_h, S_i, t)$ and $Q_{4.3}$ may be calculated from the q by the formulas (1) through (6)

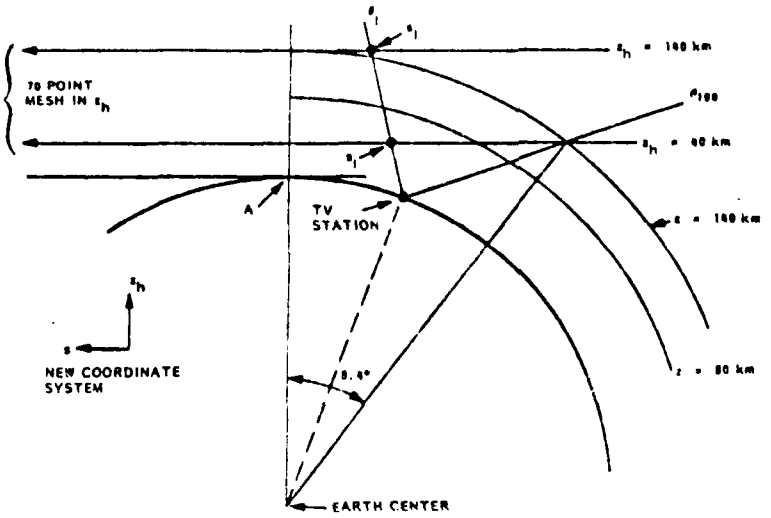

Fig. 3-6 Selection of Mesh Points for Volume Emission and Radiance Calculations

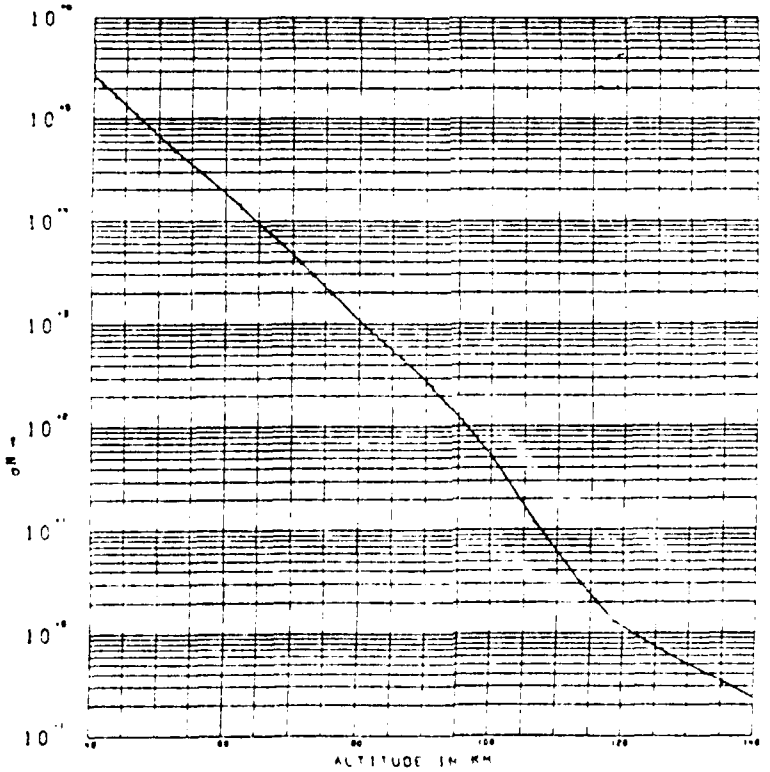

Fig. 3-7 Model for Vertical σN, Earth-Limb Viewing σN Larger Typically by a Factor 50 to 100

given previously. The values $Q_{2.7}$ and $Q_{4.3}$ must be stored back on the disc to be subsequently reread for use in the next update of $Q_{2.7}$ and $Q_{4.3}$, which occurs in processing the next pair of blue and red TV frames.

The updated values of $Q_{2.7}$ and $Q_{4.3}$ are also used to compute the volume emission $\mathcal{E}_{2.7}$ and $\mathcal{E}_{4.3}$ at 2.7 and 4.3 μm, also discussed previously. It is a simple matter to use $\mathcal{E}_{2.7}$ and $\mathcal{E}_{4.3}$ to calculate the corresponding earth-limb radiances via the formula:

$$R(x, Z_h) = \frac{1}{4\pi} \sum W_i \mathcal{E}_i$$

where W_i are weighting factors along the LOS defined by Z_h. The weighting factors are independent of postion perpendicular to the LOS. For the optically thick CO_2 4.3-μm emission the weighting factors may be given by

$$W_i = [W_b(\sigma N_i) - W_b(\sigma N_{i+})]/\sigma[CO_2]_i$$

where N_{i+} is the CO_2 column density measured from the satellite to the closest boundary of cell i, σN_{i-} is measured from the satellite to the more distant boundary of cell i, $[CO_2]_i$ is the CO_2 number density at point S_i, and the transport function W_b is defined in the paper by Kumer and James (Ref. 12). For the optically thin emissions $W_i \cong [M]^{-1} \int dS\,[M]$ across cell i, where [M] is the total atmospheric number density in units cm^{-3}.

The σN_{i+} and σN_{i-} that are used in the CO_2 4.3-μm calculation are taken from the 26 October 1978 atmospheric model for vertical σN (illustrated by Fig. 3-7) that is appropriately modified for limb viewing geometry. The quantity σN is related to vertical viewing CO_2 line center optical depth as explained in papers by James and Kumer (Ref. 13) and Kumer and James (Ref. 12). The tables for $T_b(\sigma N)$ published by Kumer and James (Ref. 12), and the limb viewing modification of the model that is shown on Fig. 3-7 are used to compute the W_i for the CO_2 4.3-μm case.

Once the $W_i(Z_h)$ are calculated for the two cases, optically thin and optically thick (CO_2 4.3 μm), they can be stored on tape and used over and over again independently of x or t. This arrangement facilitates rapid computation.

For a given auroral event, the end product of a production run will be a digital tape containing one earth-limb radiance picture per blue/red pair of TV data frames. Spatial power spectral densities for selected tangent altitudes Z_h may be computed from each IR limb radiance picture. Temporal PSDs may also be generated for selected cell positions (x, Z_h). The 2.7- and 4.3-μm auroral earth limb may be constructed from the TV data for arbitrary satellite viewing aspect. In some cases it may be useful to construct such an output tape for various satellite positions.

Section 4
SUMMARY OF THE PROJECT

Figure 4-1 shows a block diagram schematic summary of the data processing and computations which are necessary to model infrared earth-limb morphology from the blue/red TV data base.

The software has been developed to calculate radiances in limb geometry viewing for 51 horizontal LOS at each of 12 tangent altitudes from 80 to 140 km. We have chosen the LOS so that the limb viewing observations are made by looking toward magnetic west, which means we are looking parallel to the auroral oval. The lines of sight (LOS) are parallel, and 2 km apart.

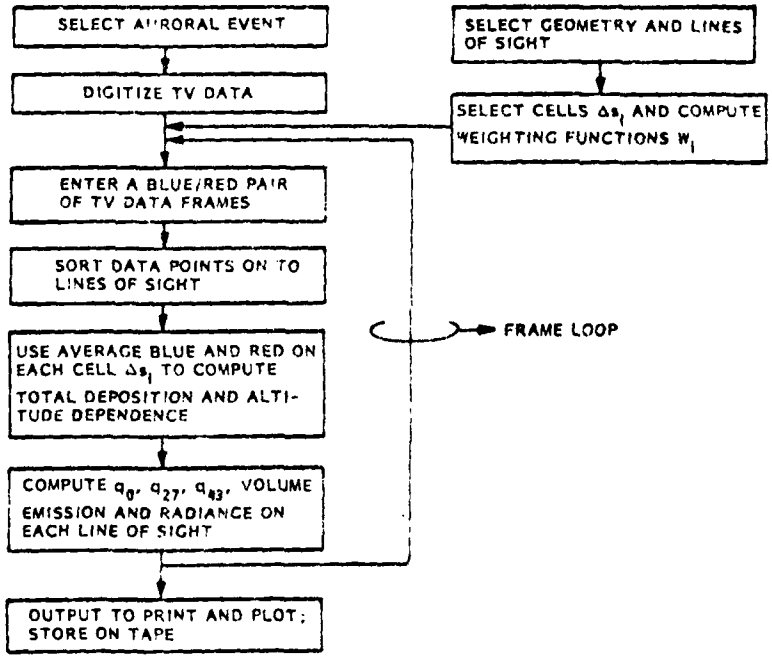

Fig. 4-1 Block Diagram Schematic Summary of the Data Processing and Computation Which are Necessary to Model Infrared Earth-Limb Morphology from the Blue/Red TV Data Base

Section 5
PRELIMINARY RESULTS

5.1 DESCRIPTION

We have now digitized and calibrated a total of ≅200 TV frame pairs of auroral TV data obtained on 23 and 27 March 1973. The event of 23 March 1973 was selected for two reasons: (1) the event included most of the phenomena listed in Table 1-1, and in fact at one point had an intensity of ≅65 Krad at 4,278 Å in significant portions of the all-sky FOV, and (2) the video tape of this event is in relatively good shape, thereby facilitating the digitization process. The video tape of the event of 27 March 1973 is also in relatively good shape, and zenith-viewing 4.3-μm measurements were obtained in that event by a radiometer mounted on a Black Brandt Rocket launched from the Poker Flat Rocket Range as part of the DNA/AFGL/USU ICECAP auroral measurements program.

In this report, we describe preliminary calculations based on the event of 23 March 1973. The calculations are performed on 100 pairs of red/blue digitized TV data frames which covered a time period of 30 minutes. The time, which was registered to the nearest 10 s, as recorded on the bar code pattern on each of the video data frames, was used to achieve the pairing of red and blue frames. The average of the two times (which were at times the same within 10 s) was used in the updating of $Q_{2.7}$ and $Q_{4.3}$ as described in Section 3.5, "Earth-limb Radiance Computation." The time between frames was 10 or 20 s for most cases.

5.2 TEMPORAL STRUCTURE

Figure 5-1 characterizes the temporal structure in limb-viewing geometry over the TV observation period. We have plotted time-dependent radiances for 2.7-μm radiance for LOS 27 for the 100 frames at tangent altitudes 105, 115, and 135 km. It can be seen that the auroral intensity was relatively weak at the beginning of the observation period at 0:43:45 local time, then increased by over an order of magnitude, then weakened in the No. 45 to No. 60 frame region.

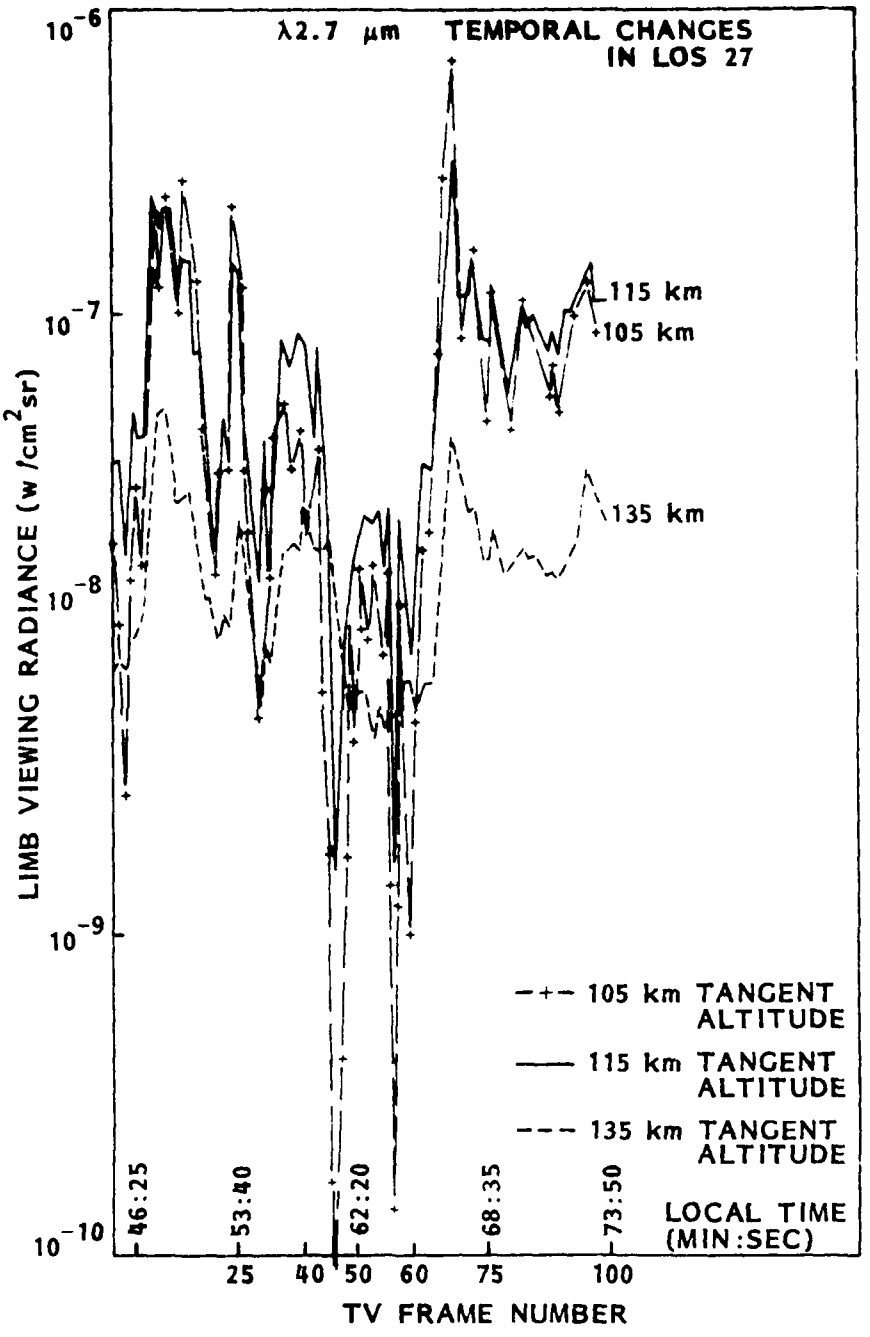

Fig. 5-1 Temporal Changes of Limb Radiance at 2.7 μm for LOS 27

Then the intensity peaked sharply, returned to a moderately high intensity and remained there until the end of the observation period at 1:13:50. High and low extremes of radiances occurred at 105 km tangent altitude. Much smaller fluctuations occurred at 135 km tangent altitutde.

Figure 5-2 shows time dependent 4.3-μm radiances for LOS 27 at a tangent altitude of 115 km. Two components of the 4.3-μm radiation due to the relatively slow varying CO_2 mechanism and to the prompt mechanism are shown. The slowly varying component rises by about a factor of 2, 3 minutes after the observations begin, then fluctuates only a few percent during the remaining 25 minutes of observation. Increases in this component are noticeably delayed from increases in auroral activity as shown by the prompt 4.3-μm radiance and by the 2.7-μm radiance shown in Fig. 5-1.

This results from the fact that the response time for the CO_2 4.3-μm aurora (something like 20 min at 115 km) is considerably longer than the response time of the $N(^2D) + O_2 \rightarrow NO(v) + O$ for 2.7=μm auroral emission, about 0.5 s at 115 km. The 26 October 1978 auroral 4.3-μm data obtained (AFGL/ USU/ DNA Auroral Measurement Program) with rocket-borne sensors with improved sensitivity indicate the presence of a 4.3-μm mechanism, very similar to the NO(V) mechanism in efficiency and in temporal behavior. Hence, this mechanism could introduce structure in the 4.3-μm earth limb well in excess of that produced by the slow CO_2 4.3-μm mechanism, as is shown in Fig. 5-2. We expect that the upcoming ELIAS earth-limb measurements will provide better definition of this mechanism. We also plan to use our blue and red all-sky TV camera to obtain data simultaneous with the 2.7- and 4.3-μm earth-limb data to be obtained in the ELIAS in order to test these hypotheses and to improve our auroral earth-limb model.

Our results from 15 selected frames have been plotted in Fig. 5-3 to give an idea of the vertical profiles of the 2.7-μm limb radiances for LOS No. 27 at 4 altitudes. From this plot it can be seen that frames No. 45 and No. 60 give the lowest limb radiances and, from the altitude of the maximum radiance and the large decrease in radiance at 100 and 105 km relative to 135-km altitude, it can be seen that the average energy of the precipitating particles is lower than for the other frames shown here.

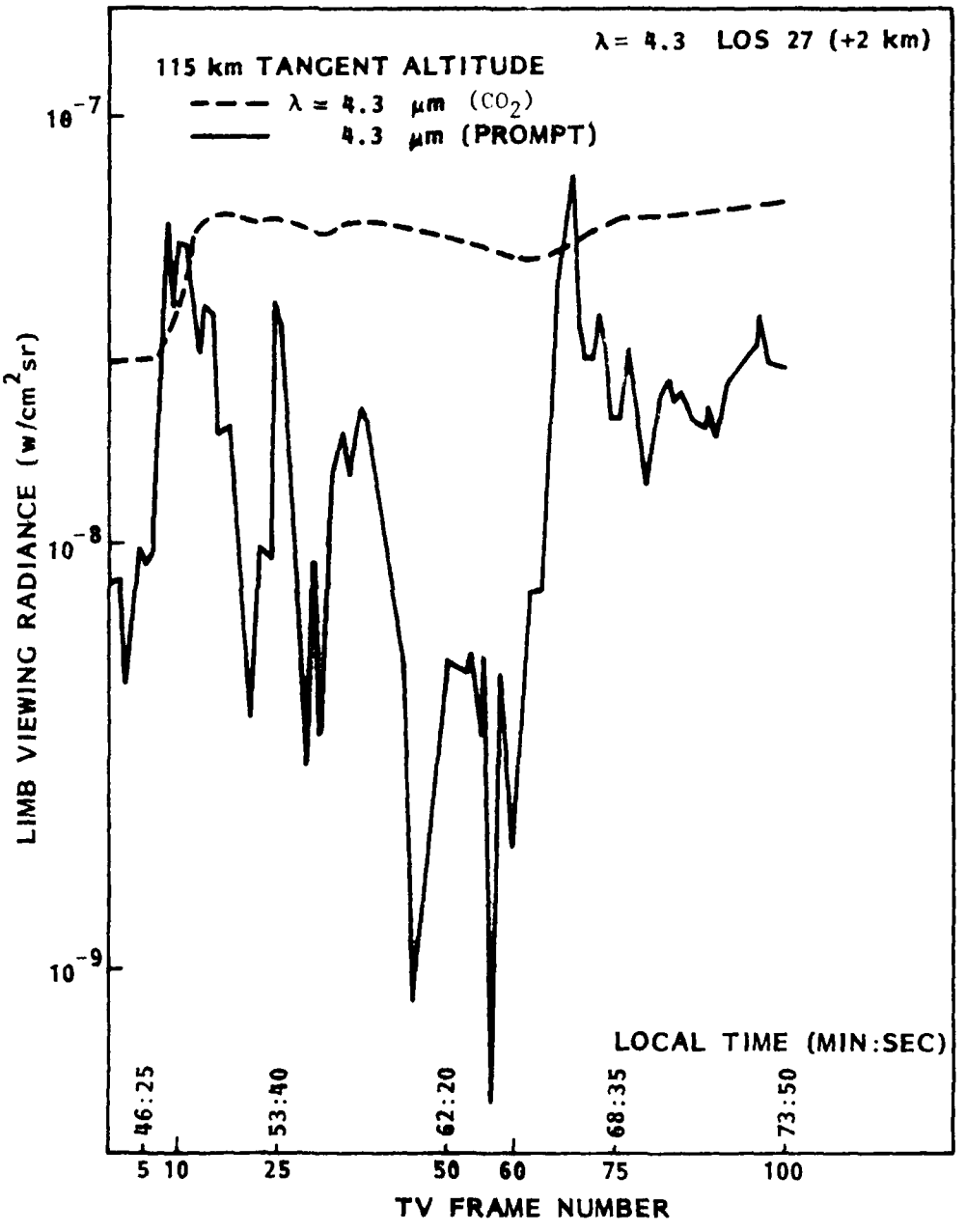

Fig. 5-2 Temporal Changes of Limb Radiance at 4.3 μm Due to the Relatively Slow CO_2 Mechanism and to the Prompt Mechanism

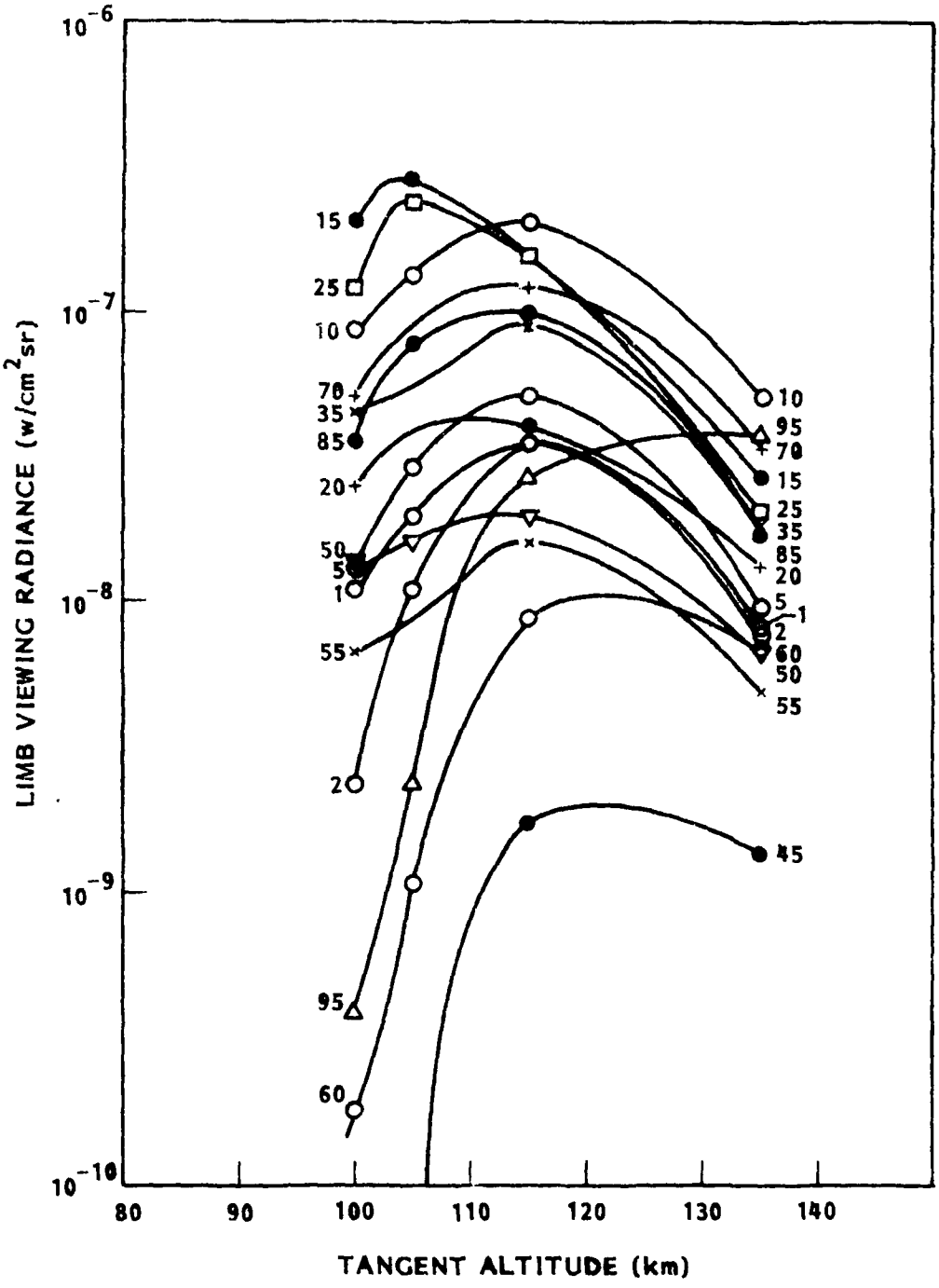

Fig. 5-3 Vertical Profiles of 2.7-μm Limb Radiance for LOS 27 for the TV Frames Indicated on the Figure

Figure 5-4 shows the calculations by Banks et al. in 1974 (Ref. 14) of ionization rate versus altitude as a function of the "hardness," or average energy, of the precipitating particles. These calculations explain and reinforce the conclusions drawn from Fig. 5-3, namely, that limb radiance at the lower tangent altitudes is a sensitive function of both total deposition and the hardness of the aurora.

To get a more complete picture of the auroral morphology during the observation period than can be obtained from the limb-viewing calculations for a selected single LOS, we have plotted in Fig. 5-5 the average auroral intensity in kilorayleighs of 4,278-Å radiation over a 20- by 20-km area near the center of the TV picture. These data were selected from the 16 by 16 pixels in the southeast and southwest quadrants at the center of the frame.

Figure 5-5 shows that the total energy deposit averaged over the two adjacent areas that approximately include 10 LOS to the East or West of the central LOS usually varied together, except in the Frame Nos. 35 to 45 region. This shows that for the frames near No. 12 and No. 68, where high auroral intensities were attained, the two large areas underwent very similar temporal fluctuations in average intensity. As is predicted by the curves of Fig. 5-4 and demonstrated by Fig. 5-3, the energy spectra for these frames are the hardest obtained among the 101 frames.

5.3 HORIZONTAL STRUCTURE

Preliminary horizontal structure data are presented for four frames (15, 20, 55, and 60) at three tangent altitudes (135, 115, and 105 km) in Figs. 5-6 through 5-11. The first two frames were selected to represent high and low auroral intensities 2.5 minutes apart (see Fig. 5-5), and the second two frames were taken in a period of low auroral intensity about 1 min, 20 s apart.

The effect of major interest in Figs. 5-6 through 5-11 is the remarkably enhanced pixel-to-pixel roughness in the prompt emissions, as compared to the relatively smooth pixel-to-pixel behaviour in the results for the slow (CO_2 4.3 μm) emission.

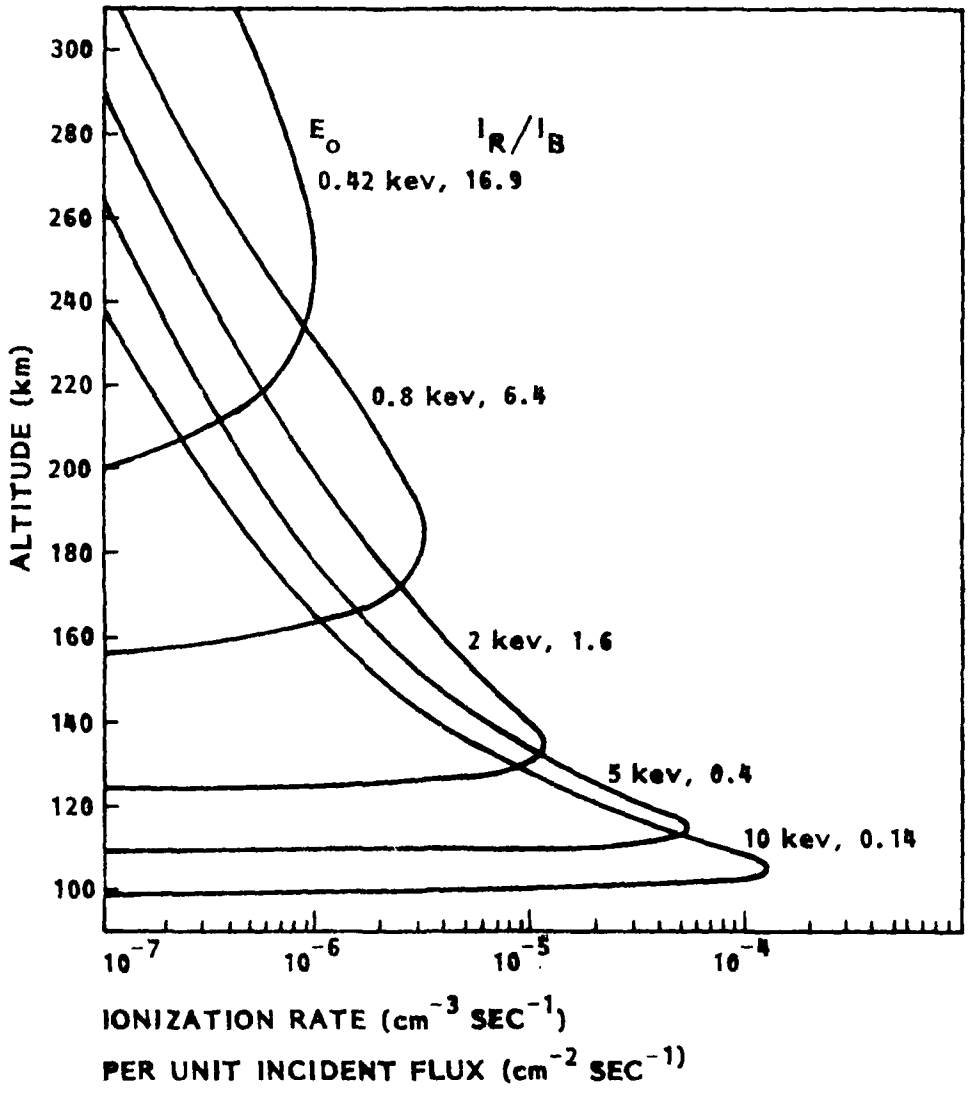

Fig. 5-4 The Vertical Profile of Ionization Rate for Unit Incident Flux of Essentially Monoenergetic Electrons in a Very Narrow Gaussian Distribution Centered on Average Energies, E_o, From 0.42 to 10 keV. Red to Blue (6,300 Å to 4,278 Å) Intensity Ratios Calculated for the Different Energy Spectra are Given on the Figure. (From Banks, et al., 1974)

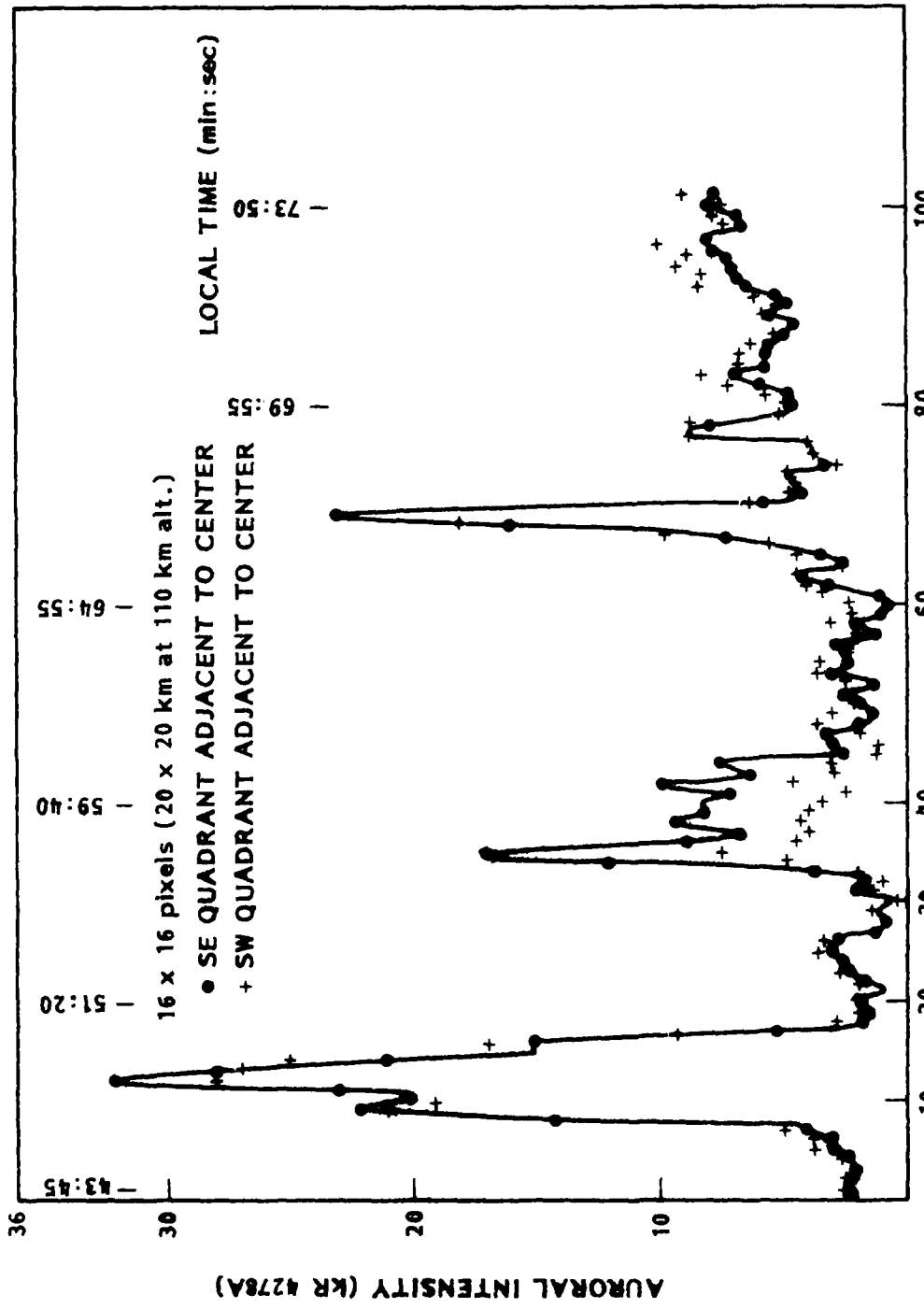

Fig. 5-5 The Time Dependence of the Average Auroral Intensity as Given by the 4,278 Å Intensity for Two 20- by 20-km Areas Adjacent to the Center of the TV Frames

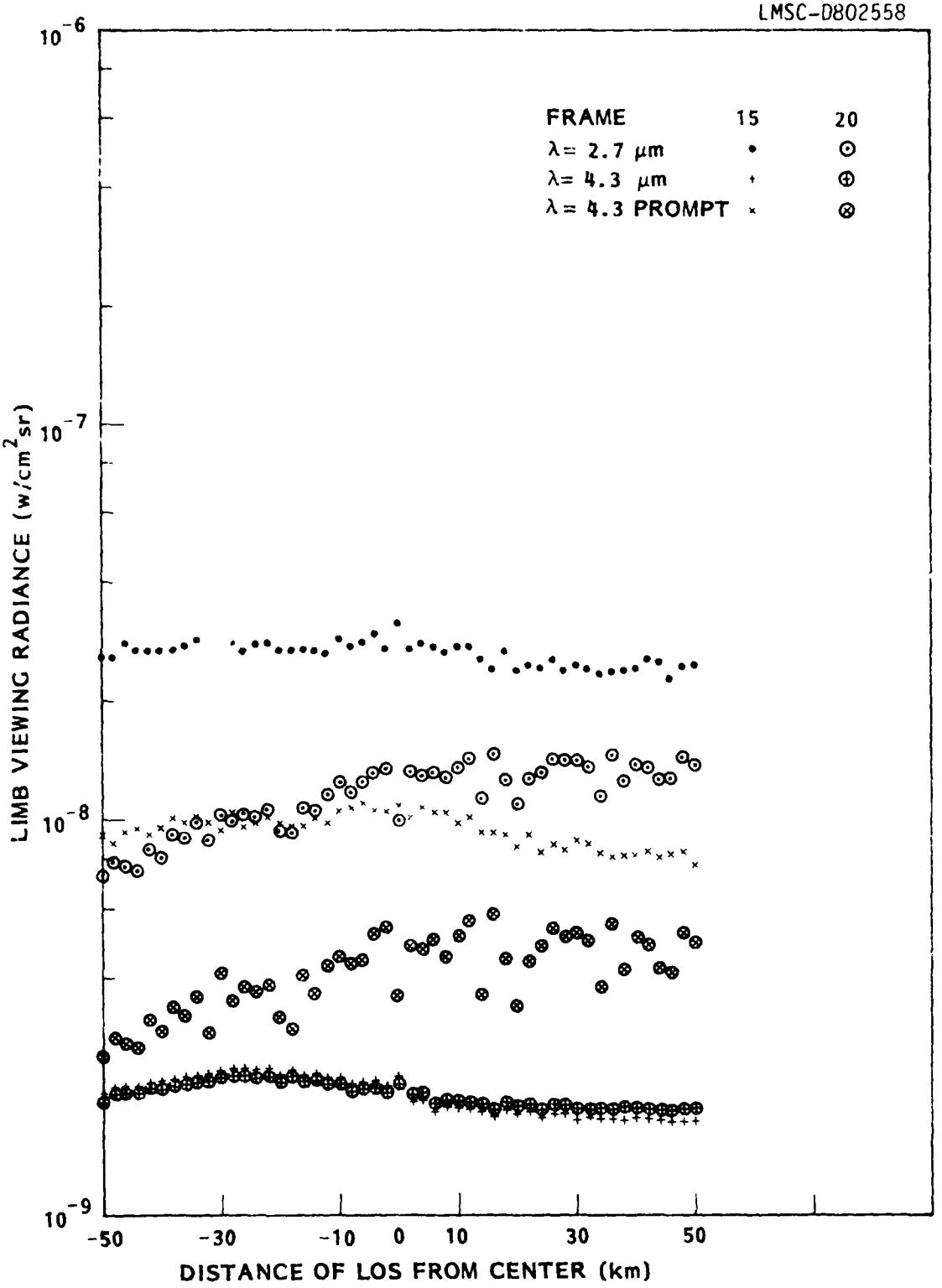

Fig. 5-6 Horizontal Structure in Limb Radiance at 135 km Altitude for Two Frames (15 and 20) About 2.5 Minutes Apart (The Average 4,278-Å Intensity Near the Center of the Scene Decreased by 1/7 Between the Two Frames)

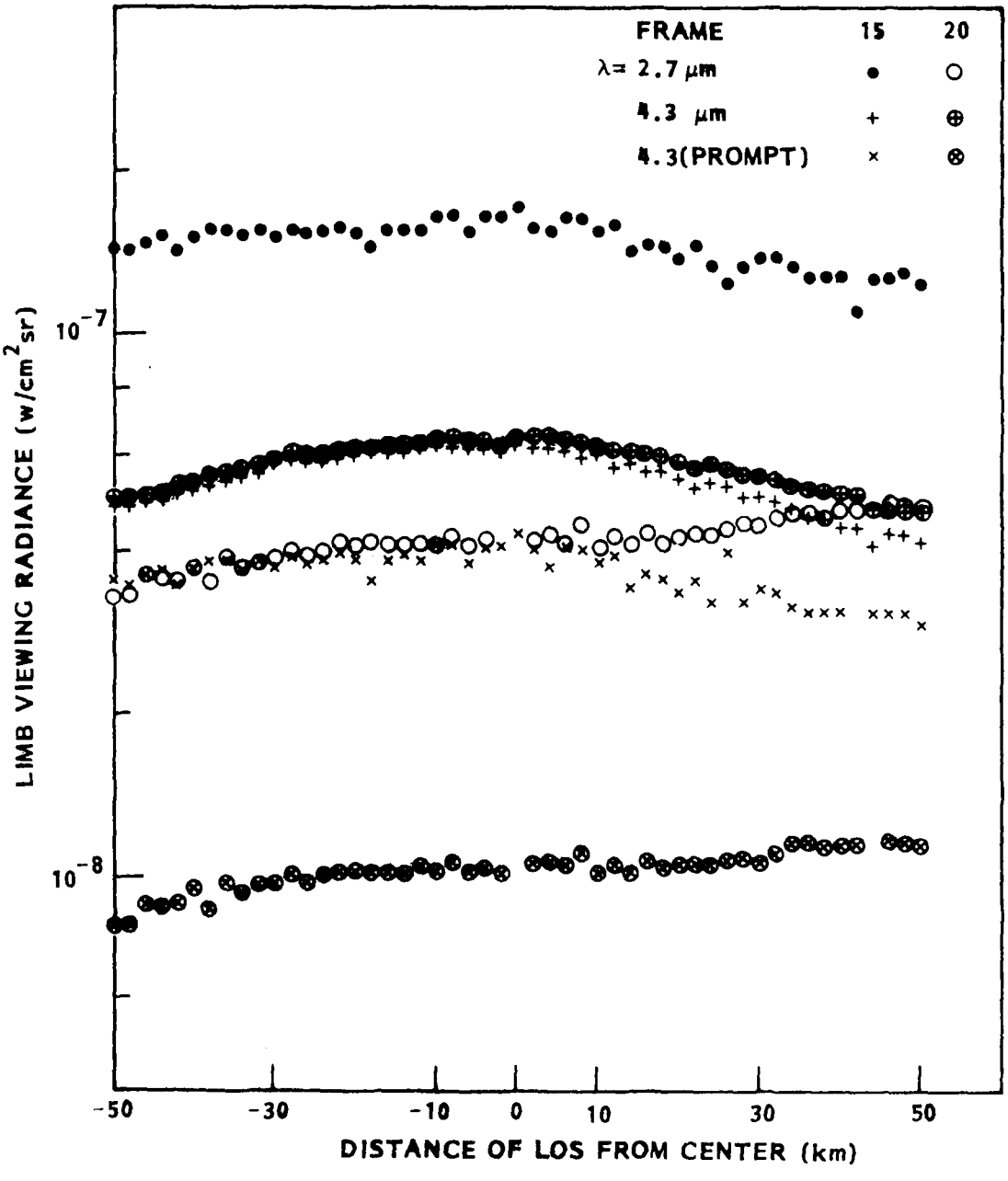

Fig. 5-7 Horizontal Structure in Limb Radiance at 115 km Altitude for Two Frames (15 and 20) About 2.5 Minutes Apart

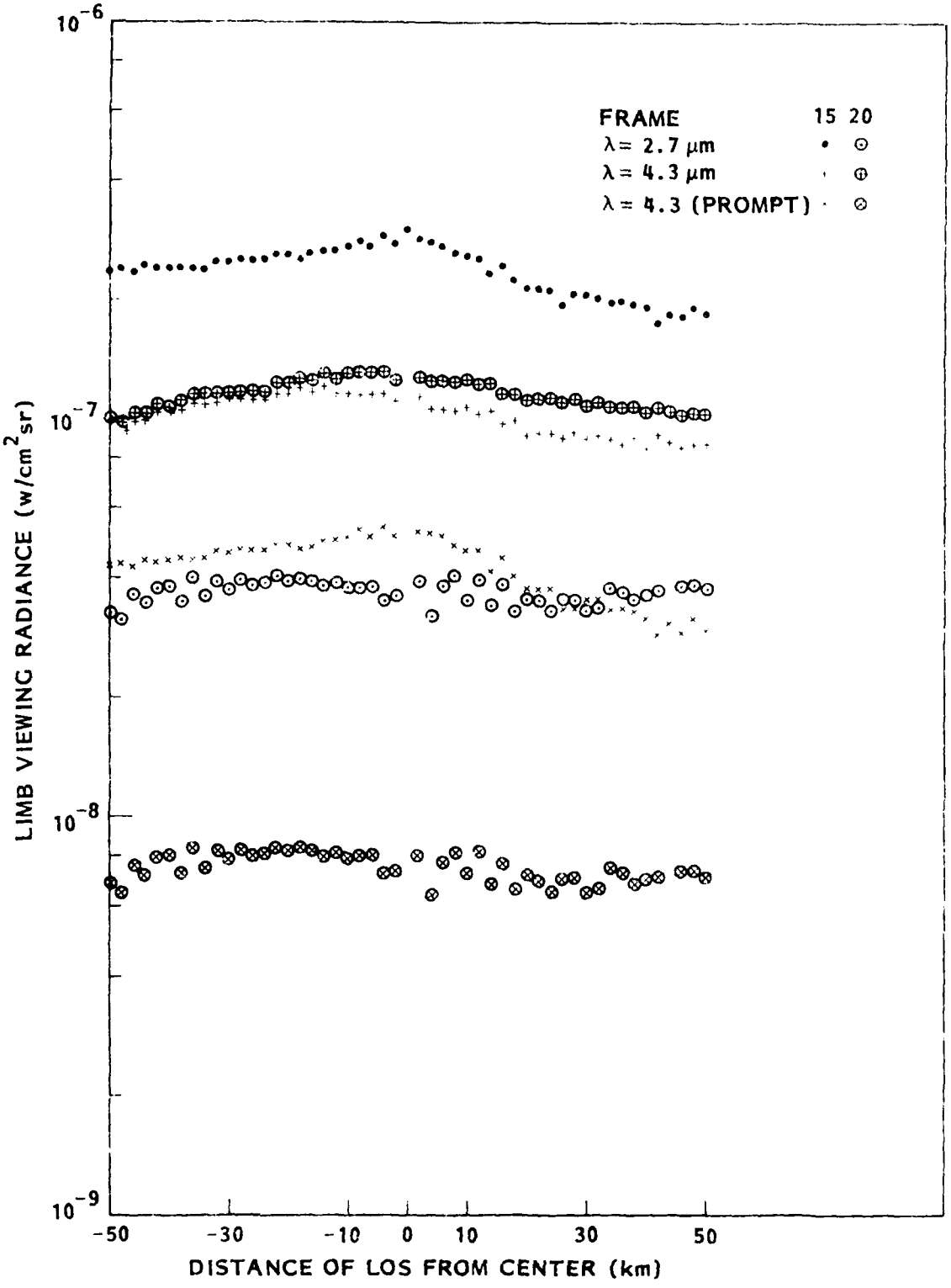

Fig. 5-8 Horizontal Structure in Limb Radiance at 105 km Altitude for Two Frames (15 and 20) About 2.5 Minutes Apart

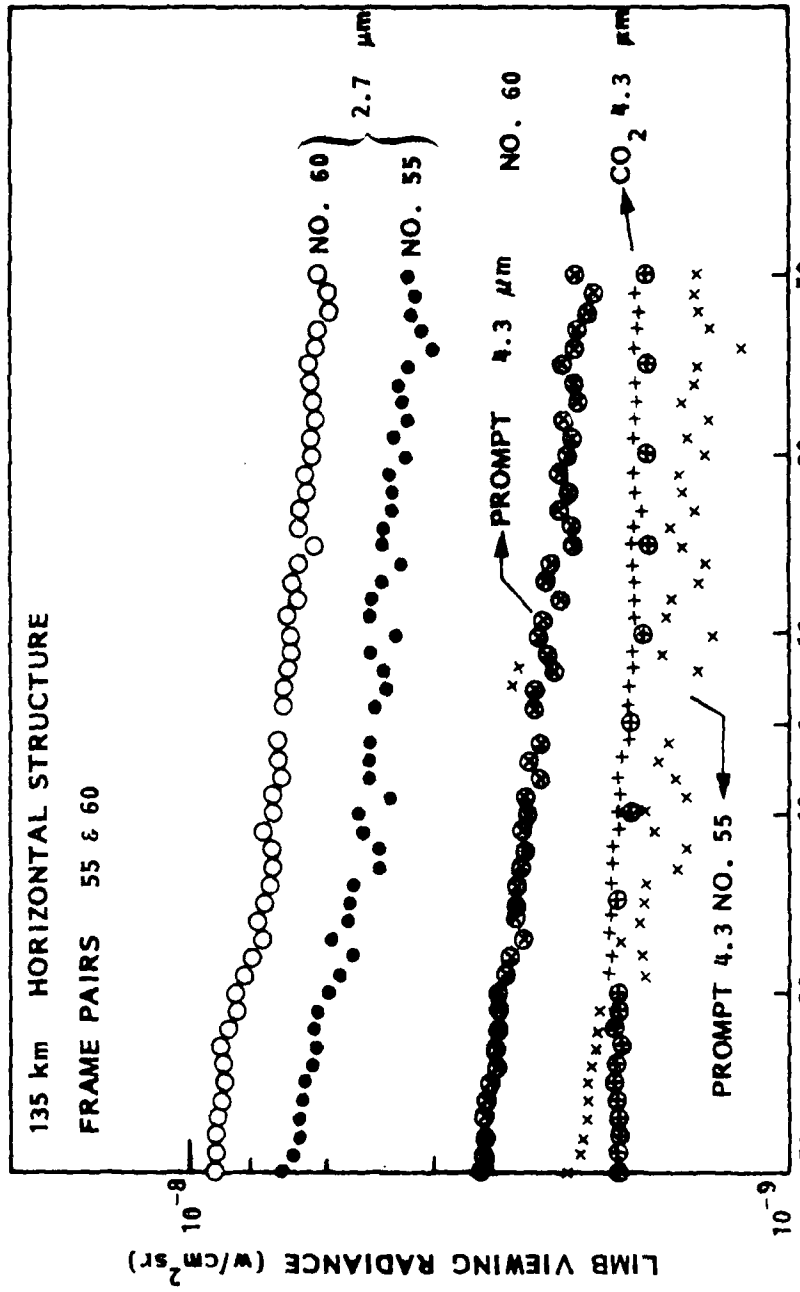

Fig. 5-9 Horizontal Structure in Limb Radiance at 135 km Altitude for Three Mechanisms for Two Frames (55 and 60) About 75 s Apart. The Average 4,278-Å Intensity Near the Center of the Scene was at a Low Level (~2 kR) and Essentially Constant Between the Two Frames

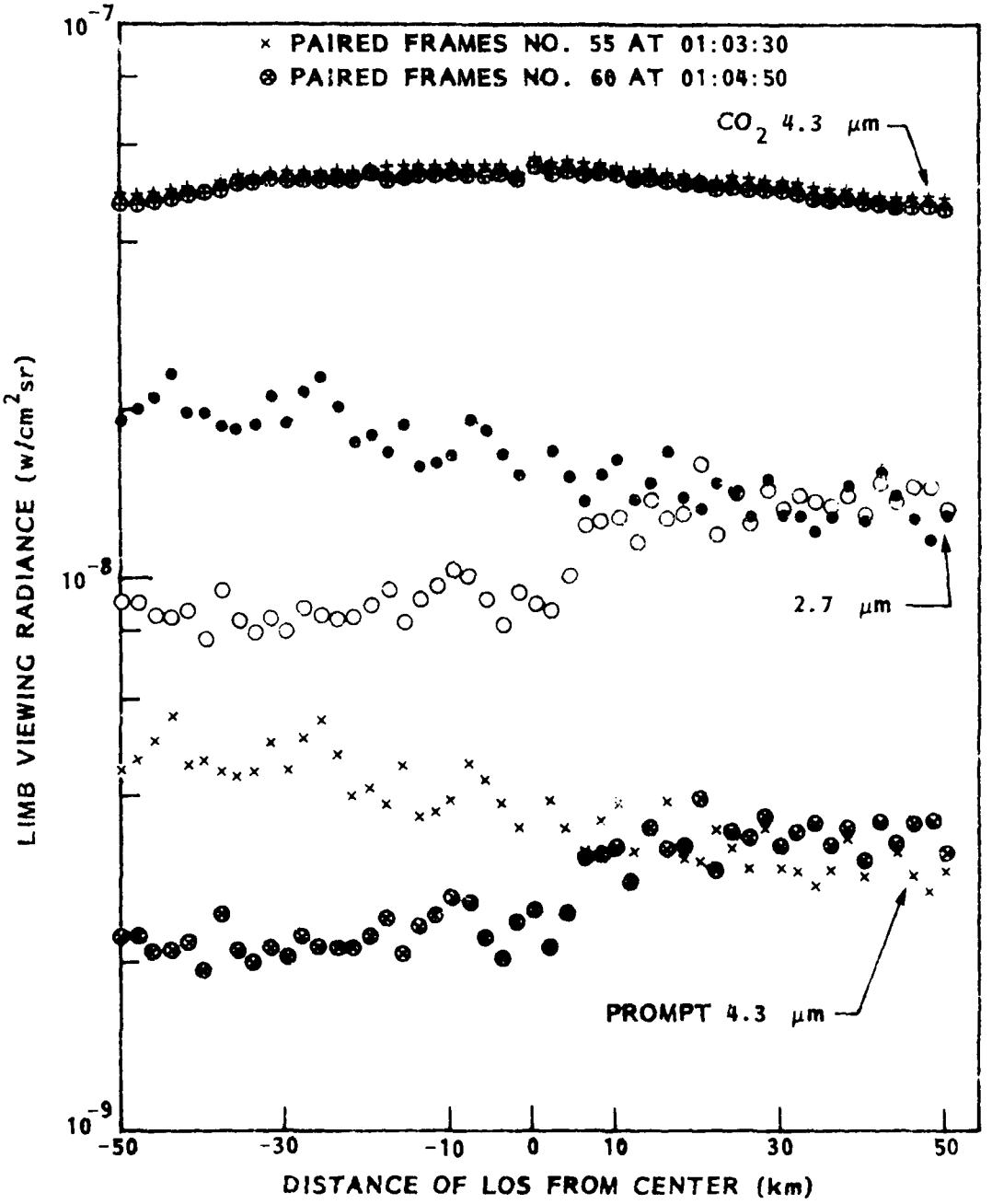

Fig. 5-10 Horizontal Structure in Limb Radiance at 115 km Altitude

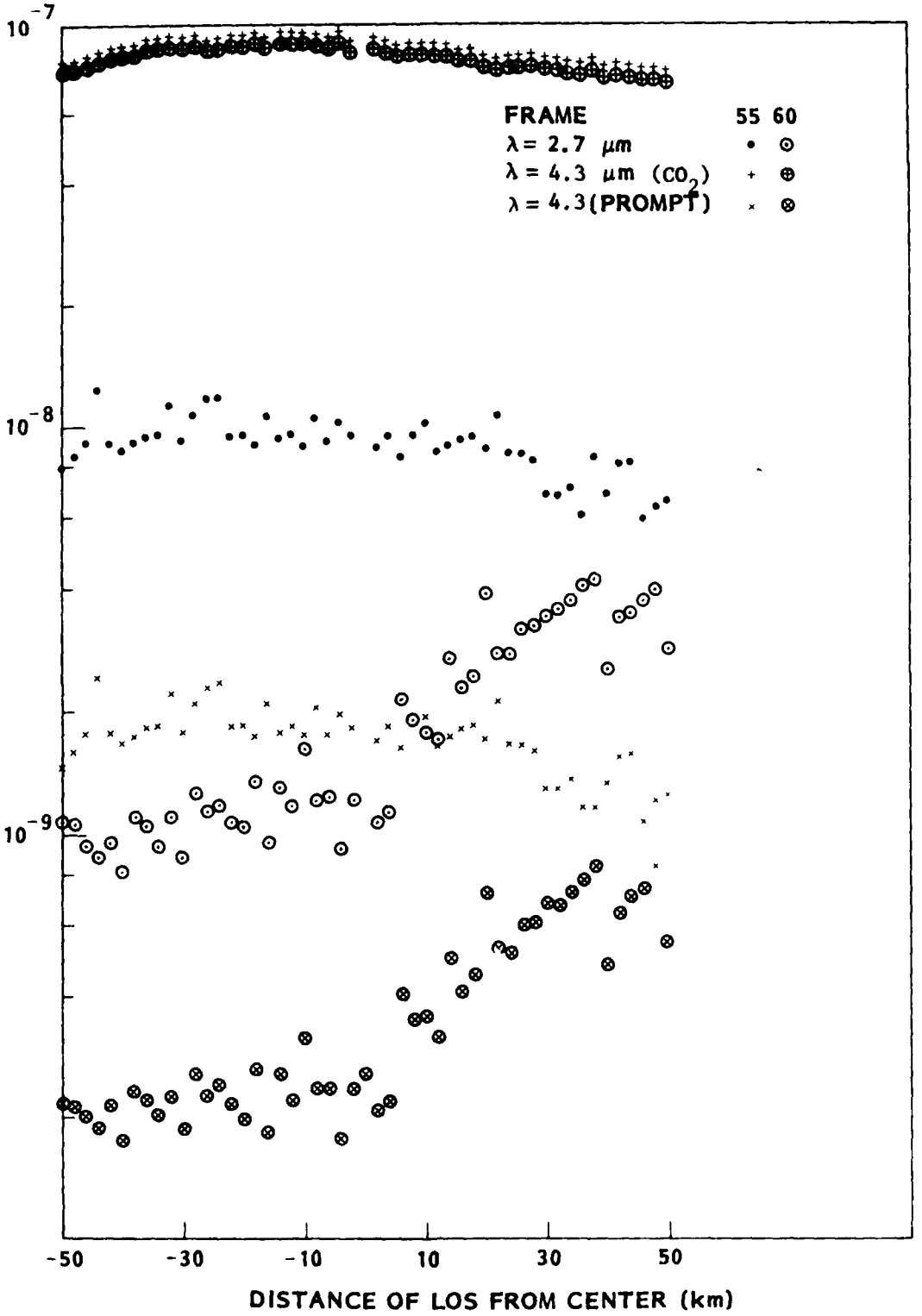

Fig. 5-11 Horizontal Structure in Limb Radiance at 105 km Altitude

The effect is most prominent for the prompt 4.3-μm radiation at 135 km tangent altitude, where pixel-to-pixel limb radiance variations were as much as 70 percent. For the 2.7-μm radiances, the maximum fluctuations were about 30 percent. Although the variations among LOS 10 km apart in the 2.7-μm and 4.3-μm (prompt) radiances were not large, the overall level for the 51 LOS for frames a few minutes apart changed almost an order of magnitude. This strengthens the conclusion reached earlier that during the observation period fluctuations in average energy precipitation were common to rather large areas.

Structure on larger scale lengths is also more prominent for the prompt emissions. For example, at the 105-km tangent altitude, Fig. 5-11 shows a case where the prompt limb radiances for the LOS to the right of the central LOS increased markedly for frame No. 60, but were about equal to those LOS on the left for frame No. 55. This effect can be seen less strongly at 115 km (Fig. 5-10) and not at all in Fig. 5-9 at 135 km. The effect is not evident for the slow CO_2 4.3-μm limb radiance. The effect is the result of a small component of more penetrating auroral particles on the right side of Figs. 5-10 and 5-11 that makes little difference in the energy deposit at 135 km or indeed in the total energy deposit.

The generally smoother variation in the slower spatial CO_2 4.3-μm limb radiances may be seen for both pairs of frames and for all three tangent altitudes where these limb radiances changed very little over the 5-frame interval even though the average energy deposition dropped by a factor of 7 in the interval over two 20- by 20-km areas containing 20 of the LOS. The 20-min time constant for the 4.3-μm radiation model accounts for this observation.

5.4 ALL-SKY TV PHOTOGRAPHS

Figures 5-12 through 5-21 present all-sky TV photographs generated from the red- and blue-filtered video data. Table 5-1 lists the frame numbers and times associated with the photographs which were selected on the basis of Fig. 5-5. The look direction used in the analysis is downward perpendicular to the

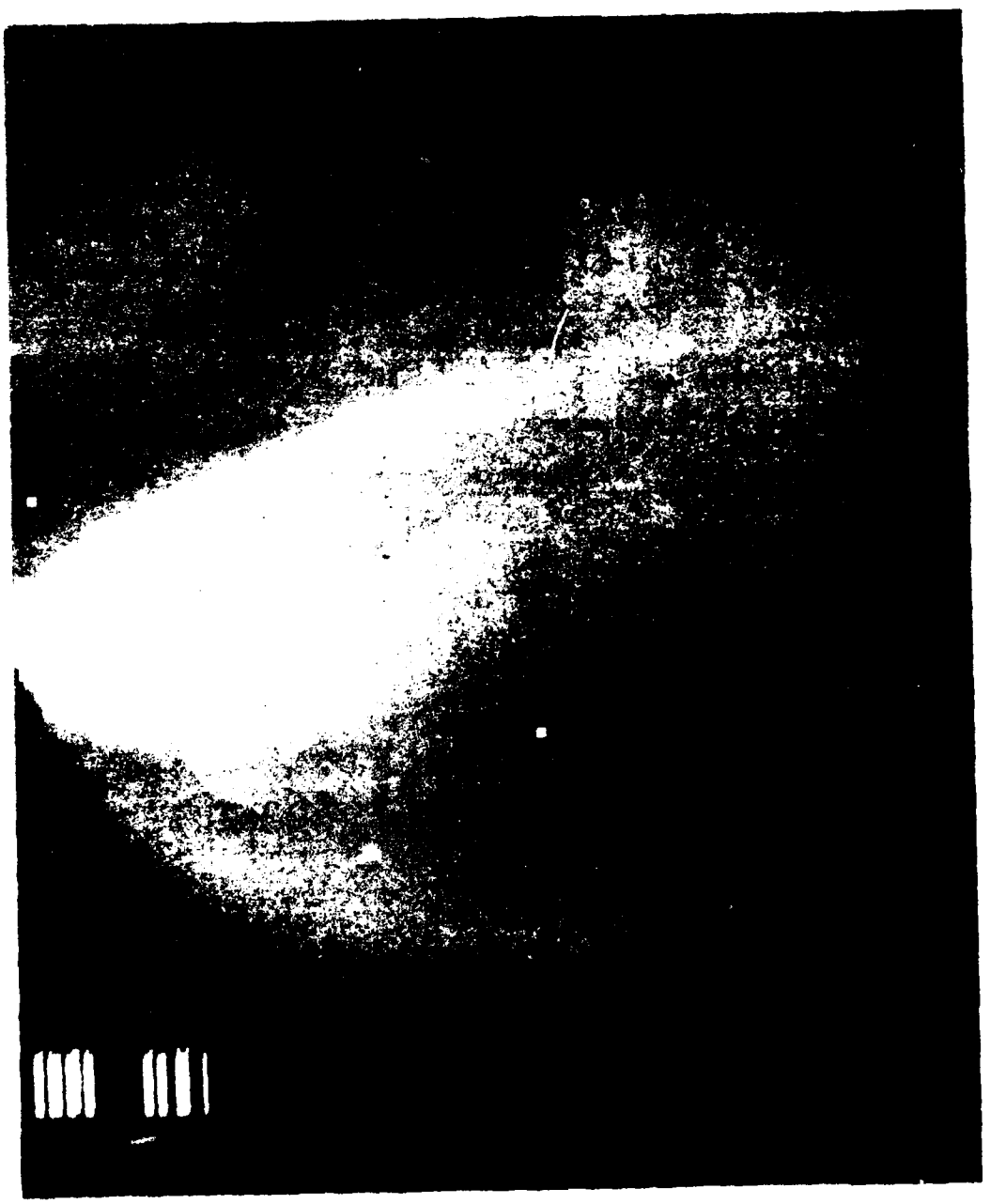

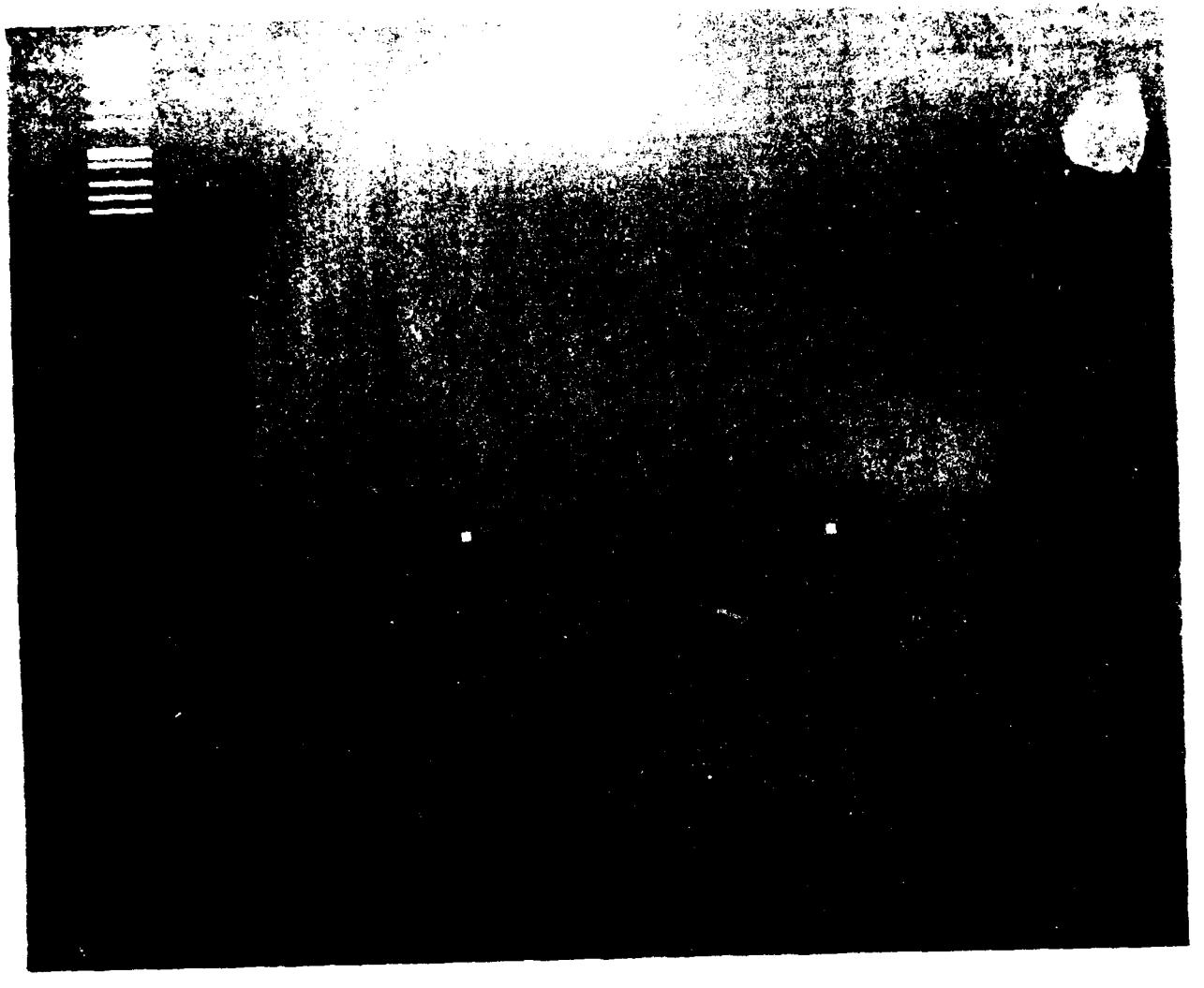

information coding bars in the upper left of the photographs. The six square index markings are on the boundaries of the area of the photographs sampled by the 51 parallel LOSs. The three markers to the left of center approximately mark LOS No. 1, where those to the right mark LOS No. 51. Because of the mapping characteristics of the all-sky camera, the observed band covers about 72 pixels near the center of the field of view (FOV), but only 26 pixels at the edges of the FOV.

Table 5-1 LIST OF FRAME PAIR NUMBERS AND TIMES OF THE PHOTOGRAPHS SHOWN IN FIGS. 5-12 THROUGH 5-21

Frame Pair Number	Red Figure No.	Time (hr:m:s)	Blue Figure No.	Time (h:m:s)	Comments
12	5-12	0:47:30	5-13	0:47:30	Highest auroral intensity
15	5-14	0:49:10	5-15	0:48:40	Large change in auroral intensity between frames
20	5-16	0:51:30	5-17	0:51:10	
35	5-18	0:58:20	5-19	0:58:20	Change in intensity between adjacent large areas
40	5-20	0:59:40	5-21	0:59:40	
55		1:3:40		1:3:40	Low level of intensity with small change in intensity between frames
60		1:4:50		1:5:00	
68		1:6:30		1:6:30	Another high intensity peak

Section 6
CONCLUSIONS

The auroral earth-limb predictions for the 23 March 1973 event that are presented here as derived from 6,300 and 4,278 Å all-sky TV data are based on facts about efficiencies and the time dependencies of the auroral NO(V) 2.7-μm and CO_2 4.3-μm mechanisms that have been well established in the AFGL/DNA Infrared Auroral Measurements program. The analysis indicates that the NO(V) 2.7-μm mechanism may be expected to produce considerably more temporal and spatial structure than the CO_2 4.3-μm mechanism.

However, the 4.3-μm region may not in fact be considerably smoother than the 2.7-μm region, since the 26 October 1978 auroral 4.3-μm data obtained (AFGL/USU/DNA Auroral Measurement Program) with rocketborne sensors with improved sensitivity indicate the presence of a 4.3-μm mechanism very similar to the NO(V) mechanism in efficiency and in temporal behavior. Hence, this mechanism could introduce structure in the 4.3-μm earth limb well in excess of that produced by the slow CO_2 4.3-μm mechanism. Our modeling of the prompt mechanism, which is based on the data obtained 26 October 1978 confirms this possibility.

We plan to use our blue and red all-sky TV camera to obtain data simultaneously with the dynamics and structure of the auroral 2.7- and 4.3-μm earth-limb data which are currently scheduled to be obtained in the ELIAS experiment in Autumn 1981. This will provide an opportunity to test and refine our models for deriving the auroral NO(V) 2.3-μm earth limb, and the relatively slow auroral CO_2 4.3-μm earth limb from red and blue all-sky TV data. Also, confirmation and refinement of our current, rather crude, model for the prompt 4.3-μm earth limb is one of the more important objectives we hope to achieve in support of the ELIAS experiment.

Section 7
REFERENCES

1. J. B. Kumer, "Further Evaluation of ICECAP Auroral 4.3 μm Zenith Radiance," Final Report on Contract DNA001-76-C-0015, HAES Report 57, 1976

2. S. B. Mende and R. H. Eather, "Monochromatic All-Sky Observations and Auroral Precipitation Patterns," J. Geophys. Res., Vol. 81, 1976, p. 3771

3. M. H. Rees and D. Luckey, "Auroral Electron Energy Derived from Ratio of Spectroscopic Emissions. 1. Model Computations," J. Geophys. Res., Vol. 79, 1974, pp. 5181-5186

4. R. D. Sears, "Characterization of the Auroral Ionosphere Using Optical Remote Sensing Techniques," paper presented at AIAA 13th Fluid and Plasma Dynamics Conference, Snowmass, Colorado, 15 July 1980

5. V. B. Wickwar, M. J. Baron, and R. D. Sears, "Auroral Energy Input From Energetic Electrons and Joule Heating at Chatanika," J. Geophys. Res., Vol. 80, 1975, p. 4364

6. R. R. Vondrak and R. D. Sears, "Comparison of Incoherent-Scatter Radar on Photometric Measurements of the Energy Distribution of Auroral Electrons," EOS Vol. 57, 1976, p. 968; J. Geophys. Res., Vol. 83, 1978, p. 1665

7. G. A. Ware et al., "Ground Support Data Report for Black Brant 18.219-1 Flight of 25 February 1974," draft report submitted to AFCRL on 2 Sep 1974

8. J. B. Kumer, "Second DNA IR Data Review Meeting Held at AFGL 10-12 April 1979," AFGL-TM-18, 1979, p. 329

9. D. J. Baker et al., "Rocketborne Measurements of Infrared Aurora and Airglow Emissions at 4.3 μm," EOS, Vol. 60, 1979, p. 328

10. J. B. Kumer, "The 4.3 μm CO_2 Aurora and Related Phenomena," J. Geophys. Res., Vol. 82, 1977, p. 2203

11. -----, "Analysis of 4.3 μm ICECAP Data," AFCRL-TR-74-0334, 1974

12. J. B. Kumer and T. C. James, "Non-LTE CO_2 and N_2 Vibrational Temperatures at 50 to 130 km Altitude," J. Geophys. Res., Vol. 79, 1974, p. 638

13. T. C. James and J. B. Kumer, "CO_2 2.7 to 4.3 μm Fluorescence: Application to Earthlimb Radiance," J. Geophys. Res., Vol. 78, 1973, p. 8320

14. P. M. Banks, C. R. Chappell and A. F. Nagy, "A New Model for the Interactions of Auroral Electrons with the Atmosphere: Spectral degradation, Backscatter, Optical Emissions, and Ionization," J. Geophys. Res., 79, 1974, pp. 1459-1470

END

DATE
FILMED

40-81

DTIC